

Improvement of Diamond-Like Carbon Adhesion on CoCrMo by Microdiamond and Nitrogen Incorporation for Wear Resistant Applications

A Thesis Submitted to the College of
Graduate and Postdoctoral Studies
In Partial Fulfillment of the Requirements
For the Degree of Master of Science
In the Department of Mechanical Engineering
University of Saskatchewan
Saskatoon
Canada

By

Jesus Corona Gomez

PERMISSION TO USE

In presenting this thesis in partial fulfillment of the requirements for a postgraduate degree from the University of Saskatchewan, I agree that the Libraries of this University may make it freely available for inspection. I further agree that permission for copying of this thesis in any manner, in whole or in part, for scholarly purposes may be granted by the professor who supervised my thesis work or, in their absence, by the College of Graduate and Postdoctoral Studies (CGPS), Head of the Department or the Dean of the College in which my thesis work was done. It is understood that any copying or publication or use of this thesis or parts thereof for financial gain shall not be allowed without my written permission. It is also understood that due recognition shall be given to me and to the University of Saskatchewan in any scholarly use which may be made of any material in my thesis.

Requests for permission to copy or to make other use of material in this thesis in whole or part should be addressed to:

Head of the Department of Mechanical Engineering
57 Campus Drive,
University of Saskatchewan
Saskatoon, Saskatchewan, S7N 5A9
Canada

OR

Dean
College of Graduate and Postdoctoral Studies
University of Saskatchewan
116 Thorvaldson Building, 110 Science Place
Saskatoon, Saskatchewan, S7N 5C9
Canada

ABSTRACT

Coating the joint surfaces with diamond like carbon (DLC) is a promising way to increase the service lifetime of hip joints made of CoCrMo alloy. DLC thin films have been attracted the most interest because of its extreme smoothness, low coefficient of friction, high hardness and excellent biocompatibility. One of the key issues that limit the use of DLC is its poor adhesion to commonly used biomedical alloys like CoCrMo. The low adhesion has been attributed to the high internal stress, and Nitrogen (N) doping is one of main approaches to minimize it. Nevertheless Nitrogen incorporation is being investigated due to the complex mechanism behind the formation of different chemical species in the amorphous DLC network by using different deposition techniques.

In the present thesis work, micro-diamond particles were synthesized on CoCrMo alloy sheets by Microwave Plasma Enhanced Chemical Vapor Deposition (MPCVD) and nitrogen doped DLC thin films were then deposited on them by Inductively Coupled Plasma assisted Chemical Vapor Deposition (ICP-CVD) to improve DLC adhesion on CoCrMo sheets. The effect of nitrogen doping and nanodiamond incorporation on the film adhesion was investigated by Rockwell indentation. Raman spectroscopy and X-ray photoelectron spectroscopy (XPS) were used to analyze the chemical structure of the coatings. Morphology of the films was observed by Scanning electron microscopy (SEM) and optical profilometry. The mechanical properties of the films were measured by nanoindentation testing. Results showed that Nitrogen doping and diamond incorporation could improve the film adhesion significantly. Raman and XPS spectra showed an increase in sp^2 bonding in N-DLC films with a consequent decrease in hardness according to nanoindentation measurements. Surface roughness decreased while nitrogen content increased according to optical profilometer images. The results have demonstrated that the modified DLC films are promising for total hip joint replacement application.

ACKNOWLEDGMENTS

I would like to express my deepest gratitude to my supervisor, Professor Qiaoqin Yang, who accepted me as her student and motivated me during my masters in science. I will always be thankful for her support, patience, advice and instruction during my master's degree.

I would like to appreciate my committee members Professor Daniel Chen and Professor Duncan Cree for their valuable advice. I would like to thank Mr. Zhao Nan Fang and Mr. Robert Peace for their assistance, training and patience during my studies.

I am very thankful with Dr. Jason Maley for Raman spectroscopy training at the Saskatchewan Structural Science Center (SSSC) and Dr. Ronny Sutarto for XPS measurements at CLS facilities, and I am grateful to my colleagues Sheida Shiri and Masoud Mohammadtaheri for their support and advice.

I highly appreciate the financial support granted by the Natural Sciences and Engineering Research Council of Canada (NSERC), the Canada Research Chair Program (CRC), and the University of Saskatchewan.

Finally, I would like to thank God, my parents and sisters for all their love, support and advice during my life.

To my beloved parents Lucila and Pedro, my sisters Erika and Lysett, and family...

TABLE OF CONTENTS

PERMISSION TO USE.....	i
ABSTRACT	ii
ACKNOWLEDGMENTS	iii
TABLE OF CONTENTS.....	iv
LIST OF TABLES.....	vi
LIST OF FIGURES	vii
ACRONYMS.....	ix
CHAPTER 1 – INTRODUCTION	1
1.1 Motivation	1
1.2 Objectives.....	2
1.3 Thesis Organization.....	3
CHAPTER 2 - LITERATURE REVIEW.....	4
2.1 Overview of CoCrMo alloy	4
2.2 Carbon materials	6
2.3 Diamond Like Carbon Thin Films	9
2.3.1 Structure and Properties of DLC.....	9
2.3.2 DLC deposition techniques.....	11
2.3.3 Deposition Mechanism	13
2.3.4 Stresses in DLC	15
2.4 Adhesion improvement of DLC on CoCrMo	18
2.5 Doping of DLC	18
2.6 Nitrogen doped DLC	20
2.6 Structural characterization of DLC thin films	22
2.6.1 Raman spectroscopy	22
2.6.3 X-ray photoelectron spectroscopy	23
2.7 Mechanical characterization	25
2.7.1 Nanoindentation.....	25
2.7.2 Rockwell C indentation.....	27
2.7.3 Scratch test.....	28
2.7.4 Friction and Wear resistance.....	28
CHAPTER 3 – MATERIALS AND METHODS	30
3.1 Thin Film Deposition.....	30
3.1.1 MPCVD System	30
3.1.2 Chemical Vapor Deposition System.....	31
3.2 Structural Characterization	34

3.3 Surface Morphology	35
3.4 Mechanical testing	37
3.5 Tribological Characterization	38
CHAPTER 4 – RESULTS AND DISCUSSION	40
4.1 Adhesion Enhancement of DLC on CoCrMo Alloy by Microdiamond particles and Nitrogen Incorporation.	40
4.1.1 Chemical Characterization.....	40
4.1.2 Surface Morphology	43
4.1.3 Surface Profilometry.....	43
4.1.4 Mechanical Properties.....	44
4.1.5 Adhesion	45
4.2 Effect of nitrogen content on tribological properties of D/NDLC films on CoCrMo alloy.....	46
4.2.1 Chemical Bonding and Structural Characterization.....	46
4.2.2 Surface Topography.....	51
4.2.3 Mechanical Properties.....	52
4.2.4 Adhesion	52
4.2.5 Friction and Wear	54
CHAPTER 5 - CONCLUSIONS AND FUTURE WORK RECOMMENDATIONS	57
5.1 Summary and Conclusions	57
5.3 Future work.....	57
REFERENCES	59

LIST OF TABLES

Table 2.1 Composition of CoCrMo ASTM F-1537 [25]	5
Table 2.2 Properties of CoCrMo ASTM F-1537 [25]	6
Table 3.1 Deposition parameters employed in DLC and NDLC films	34
Table 4.1 Hardness and Young's modulus of CoCrMo, DLC and D-NDLC coatings	45
Table 4.2. Binding energies of the different chemical states on DLC, D-NDLC-1, and D-NDLC-4..	50
Table 4.3. Hardness, Young's modulus of CoCrMo, DLC and ND-NDLC coatings	52
Table 4.4 Wear rate values for UHMWPE balls against DLC and NDLC coatings	56

LIST OF FIGURES

Figure 2.1 Injured hip joint and its artificial replacement[24]	4
Figure 2.2 Ground state of Carbon	6
Figure 2.3 sp configuration of Carbon.....	7
Figure 2.4 sp ² configuration of Carbon	7
Figure 2.5 sp ³ configuration of carbon.....	8
Figure 2.6 Different atomic structures of carbon: a) Graphite, b) Diamond, , c) C60 (Buckminsterfullerene), d) Single-wall carbon nanotube, and e) Graphene[33].	9
Figure 2.7 Ternary phase diagram of amorphous carbon with different sp ² , sp ³ and H content [35]...	10
Figure 2. 8 Molecular dynamic simulation of atomic structure of a-C:H film [37].....	11
Figure 2.9 Diagrams of different DLC deposition techniques[35].	12
Figure 2.10 Growth mechanism of a-C:H[35].	15
Figure 2.11 Idealized behavior of intrinsic stress with different impact energy per atom[50].	17
Figure 2.12 Scheme of known DLC dopants to improve particular properties[37].....	19
Figure 2.13 Different Nitrogen-Carbon configurations[35].	20
Figure 2. 14 Cross-linking of graphitic structures with formation of pentagons by increasing nitrogen concentration in the films from a) 5% to b) ~15%[57].	21
Figure 2.15 Raman spectra comparison of diamond and amorphous carbon structures [35].	23
Figure 2.16 Schematics of the excitation, photoemission and Auger processes [69].	24
Figure 2.17 Typical loading unloading graph for ta-C:H Nano-hardness test[77]	26
Figure 2.18 Schematics of different adhesion stages according to VDI 3891 guideline[82].....	27
Figure 2.19 Schematic image of scratch test[84].....	28
Figure 2.20 Schematic image of a Ball-on-disk configuration.	29
Figure 3.1 Photograph of MPCVD System	31
Figure 3.2 Schematic of PECVD.....	32
Figure 3.3 Photograph of plasma enhanced chemical vapor deposition system.....	33
Figure 3.4 Reinshaw 2000 Raman spectroscope	35
Figure 3.5 Picture of Zygo NewView Optical profilometer	36
Figure 3.6 Picture of JOEL JSM 6010 LV Scanning electron microscopy	36
Figure 3.7 Picture of Universal Mechanical Tester for nano-indentation investigation	37
Figure 3.8 Rockwell C indenter	38
Figure 3.9 UTM (left) and Ball-on-disk configuration for friction and wear tests (right).....	39

Figure 4.1 Raman spectra of micro-diamond particles on CoCrMo alloy	41
Figure 4.2 SEM of deposited micro-diamond particles on CoCrMo alloy	41
Figure 4.3 Raman Spectra of (a) DLC and (b) NDLC on silicon	42
Figure 4.4 Raman Spectra of (a) D/DLC and (b) D/NDLC on CoCrMo alloy	42
Figure 4.5 SEM images of (a) DLC delamination and (b) D-DLC on CoCrMo alloy	43
Figure 4.6 Surface Roughness of bare and coated CoCrMo alloys	44
Figure 4.7 SEM images after Rockwell C indentation of (a) DLC on bare CoCrMo alloy, (b) D-DLC on CoCrMo alloy and (c) D-NDLC on CoCrMo alloy	46
Figure 4.8 Raman spectra NDLC coatings on silicon with a) 0sccm, b) 4sccm, c) 8sccm, d) 12 sccm and e)16 sccm Nitrogen flow rate	47
Figure 4.9 Raman spectra NDLC coatings on micro-diamond CoCrMo alloys with a) 0sccm, b) 4sccm, c) 8sccm, d) 12 sccm and e)16 sccm Nitrogen flow rate	48
Figure 4.10 XPS C1s spectra of DLC on silicon	49
Figure 4.11 De-convolution of C1s XPS spectra of a) D-NDLC-1, and b) D-NDLC-4.....	49
Figure 4.12 De-convolution of N1s XPS spectra of a) D-NDLC-1, and b) D-NDLC-4	50
Figure 4.13 RMS Roughness of DLC and nitrogenated DLC films on CoCrMo alloys	51
Figure 4.14 SEM images after Rockwell C indentation of a) DLC, b) D-DLC-1, c) D-NDLC-2, d) D- NDLC-3, and d) D-NDLC-4.	54
Figure 4.15 Coefficient of Friction of DLC and NDLC films against UHMWPE balls.....	55
Figure 4.16 SEM images of wear tracks on D-DLC and D-NDLC-4 samples, the white areas correspond to UHMWPE balls loss	56

ACRONYMS

a-C	Amorphous Carbon
a-C:H	Hydrogenated amorphous carbon
DLC	Diamond-Like Carbon
C60	Buckminsterfullerene
C540	Icosahedral fullerene
C70	Fullerene-C70, rugbyballene
CVD	Chemical Vapor Deposition
PVD	Physical Vapor Deposition
MSIB	Mass Selected Ion Beam
FCVA	Filtered Cathodic Vacuum Arc
PLD	Pulsed Laser Deposition
PECVD	Plasma Enhanced Chemical Vapor Deposition
σ	Residual stress
σ_{th}	Thermal stress
σ_i	Intrinsic stress
σ_e	Extrinsic stress
ϕi	Ion flux
ϕd	Deposition rate
PBS	Phosphate-buffered saline
BWF	Breit-Wigner-Fano
XPS	X-ray photoelectron spectroscopy
E_k	Kinetic energy
$h\nu$	Photon energy
E_B	Binding energy
ISE	Indentation size effect
H	Hardness
h_p	Plastic deformation
L_{max}	Maximum load,
h_{max}	Maximum indent
E	Young's modulus
MPCVD	Microwave Plasma Chemical Vapor Deposition
UTM	Universal Testing Machine
UHMWPE	Ultra-high molecular weight polyethylene
RMS	Root Mean Squared
COF	Coefficient of Friction

CHAPTER 1 – INTRODUCTION

1.1 Motivation

One of the most critical and international public health issues is hip joint fracture [1]. The main cause of hip joint fracture is degeneration of the bones [2]. Limited mobility, hospital and social costs, and impairment in quality of life are some implications of hip joint fracture [3]. Total hip replacement, in which the head of the femur and its socket are replaced, is the main procedure to re-establish functions of fractured hips. The life time of the implants strongly depends on the design and quality of the materials used [4].

One of the most common materials used for hip joint replacement is CoCrMo alloy because of its good corrosion and wear resistance, biocompatibility, and high strength. CoCrMo alloys comply the ASTM standard of F-75 for casting alloys and F-1537 for wrought alloys for surgical implants [5]. Over time, the implants become loose and release toxic ions due to the wear between moving surfaces and the corrosion in human fluids, which makes the implants fail [5]. In order to reduce the ion release and extend the life time of the implant, surface modification and coating have been investigated. Coatings can enhance surface characteristics and mechanical performance without altering the bulk properties of the implants and very promising to improve both the performance and the lifetime of the implants [6].

Diamond like Carbon (DLC) thin films have been attracted the most interest because of its extreme smoothness, low coefficient of friction, high hardness and excellent biocompatibility [7-9]. One of the key issues that limit the use of DLC is its poor adhesion to commonly used biomedical alloys like CoCrMo alloy [10]. The low adhesion has been attributed to the high internal stress of DLC due to the ion bombardment, and weak interface between the substrate and coating. Surface substrate modification, interlayer between the substrate and coating, and doping elements into the coating to reduce internal stress are the main approaches to increase DLC adhesion [11–15].

Surface treatment with nitrogen plasma on CoCrMo alloy has formed a passive layer at low temperature with good corrosion resistance of DLC coatings but with a negative effect on tribology performance [16]. Further studies were performed by using a hip joint simulator wear test, concluding that neither nitrogen ion implantation nor pure DLC coatings can enhance wear

resistance of CoCrMo on polyethylene polymer for hip joint implant application[17]. Titanium interlayer deposited after nitrogen ion implantation on CoCrMo has improved surface hardness and wear resistance, but weak adhesion was observed[18]. A detailed X-ray photoelectron spectroscopy (XPS) analysis reported a formation of cobalt carbide at the less than 5 nm interface between the substrate and DLC coating, and suggested that metastable cobalt carbide might lower DLC adhesion[19].

Recent studies have reported that diamond incorporation on Titanium alloys can enhance the interface with DLC and increase its adhesion[20,21]. Reduction of internal stress has been achieved by nitrogen doping DLC deposited on silicon, steel and glass substrates[22,23]. Consequently, the combination of diamond particles deposited on CoCrMo and nitrogen doped DLC deposition can be very promising for adhesion improvement and wear resistance of CoCrMo on polyethylene for artificial hip joint replacement.

1.2 Objectives

The primary objective of the present thesis work is to improve adhesion of DLC on CoCrMo alloy. In order to accomplish this goal, specific sub-objectives include the following:

1. Improve DLC adhesion on CoCrMo alloys by microdiamond particle deposition by Microwave Plasma Chemical Vapor Deposition.
2. Deposit nitrogen doped DLC coatings with different nitrogen content on diamond predeposited CoCrMo samples by Plasma-Enhanced Chemical Vapor Deposition.
3. Analyze the chemical structure and morphology of N-DLC samples at different nitrogen concentrations.
4. Measure the mechanical and tribological properties of the coatings, to understand the relationship between chemical structure and properties of the synthesized films.

1.3 Thesis Organization

Chapter 1 covers motivation and objectives of the present research work and the organization of the present thesis.

Chapter 2 presents a comprehensive review of CoCrMo alloy and DLC coatings. This chapter explains the chemical nature of carbon bonds, defines DLC and its properties, and describes the deposition techniques and mechanism of DLC growth.

Chapter 3 introduces the experimental techniques and parameters used in this research related with deposition and characterization of the coatings.

Chapter 4 consists in two sections. The first section 4.1 shows the results of adhesion improvement by diamond and nitrogen incorporation with an analysis of bonding structure, morphology and mechanical properties. The second section 4.2 explains further the effect of nitrogen doping DLC at different concentrations on chemical structure, morphology, adhesion, mechanical and tribological properties.

Chapter 5 concludes the results presented in Chapter 4, and suggests direction for future work on this topic.

CHAPTER 2 - LITERATURE REVIEW

Due to the extreme smoothness, low coefficient of friction, high hardness and excellent biocompatibility Diamond like Carbon (DLC) thin films have been attracted the most interest for biomedical applications[1-3] such as hip joint replacement. One of the key issues that limit the use of DLC is its poor adhesion to commonly used biomedical alloys like CoCrMo [10]. This chapter will provide a comprehensive review on CoCrMo alloy, diamond-related carbon materials structure and deposition techniques, diamond based coatings on CoCrMo, and principles and descriptions of characterization techniques.

2.1 Overview of CoCrMo alloy

Globally, one of the most severe and public health issues is hip joint fracture [1]. The main cause of hip joint fracture is degeneration of the bones [2]. Restricted mobility, hospital and social expenses, and decay in quality of life are some implications of hip joint fracture [3]. Total hip replacement, in which the head of the femur and its socket are replaced, is the main procedure to re-establish functions of fractured hips.



Figure 2.1 Injured hip joint and its artificial replacement[24]

The life time of the implants strongly depends on the design and quality of the materials used [4]. One of the most common materials used for hip joint replacement is CoCrMo alloy as a femoral head while Ultra High Molecular Weight Polyethylene (UHMWP) is used as a liner for the cup, both materials are in contact. CoCrMo has been widely used as the head for hip joint replacement because of its good corrosion and wear resistance, biocompatibility, and high strength. CoCrMo alloys comply the ASTM standard of F-75 for casting alloys and F-1537 for wrought alloys for surgical implants [5]. Table 2-1 shows the composition and Table 2-2 shows the magnitude of selected properties of CoCrMo ASTM F-1537 alloy [25] which was used in the present studies.

Table 2.1 Composition of CoCrMo ASTM F-1537 [25]

Element	Composition (Wt%):
C	0.05
Mn	0.83
Si	0.64
P	0.003
S	0.0005
Cr	27.82
Ni	0.07
Mo	5.48
Cu	0.01
Co	64.68
N	0.163
W	0.02
Fe	0.14

Table 2.2 Properties of CoCrMo ASTM F-1537 [25]

Tensile	Yield	Elongation	Reduction
Strength [MPa]	Strength [MPa]	[%]	of Area [%]
1338.0	965.0	31.0	25

Over time, the implants become loose and release toxic ions due to the wear between moving surfaces and the corrosion in human fluids, which makes the implants fail [5]. In order to reduce the ion release and extend the life time of the implant, surface modification and coating have been investigated.

2.2 Carbon materials

Among other elements in the periodic table, carbon is one of the most abundant elements and principal component of earth's life. Carbon can form different covalent bonds using its four valence electrons of 2s and 2p atomic orbitals.

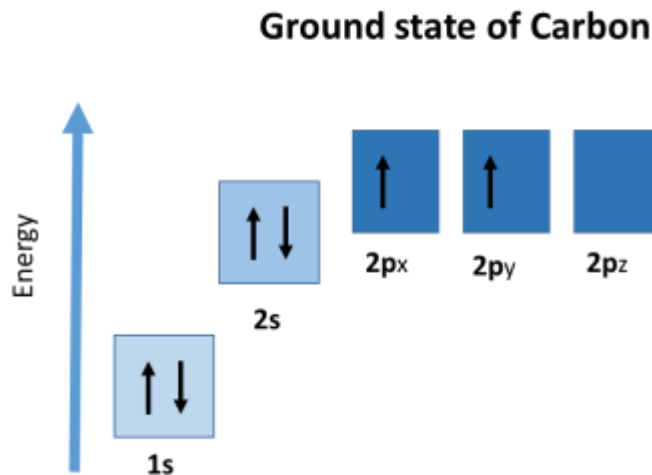


Figure 2.2 Ground state of Carbon

The combination of 2s and 2p orbitals originates the hybrid orbitals sp , sp^2 and sp^3 . Figure 2.3 shows the sp configuration. When 2s orbital combines with one of the 2p orbitals, the hybridization results in 2 sp -orbitals. This configuration allows forming triple bonds with other carbons of the same configuration (alkynes).

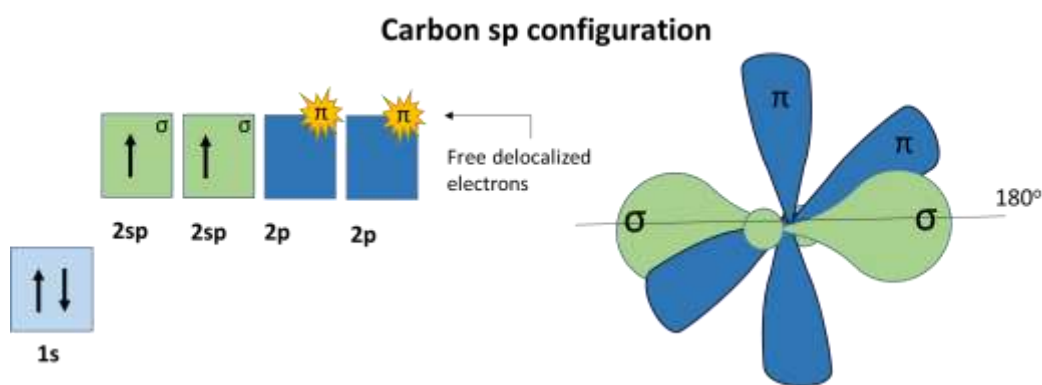


Figure 2.3 sp configuration of Carbon

Sp^2 hybridization takes place when two 2p orbitals mix with 2s orbital, resulting in 3 sp^2 -orbitals and one p orbital. The 3 sp^2 orbitals are in the same trigonal plane with an angle of 120° among them. A hexagonal arrangement of this sp^2 configuration originates graphene in a single atom plane. The remaining 2p orbital can form a weak Van der Waals bond with another 2p orbital from another plane, the accumulation of many planes with these weak π bonds forms graphite. Graphite is soft, it can be used as a dry solid lubricant, and its free electron migrates along the plane making it a good electrical conductor[12,13].

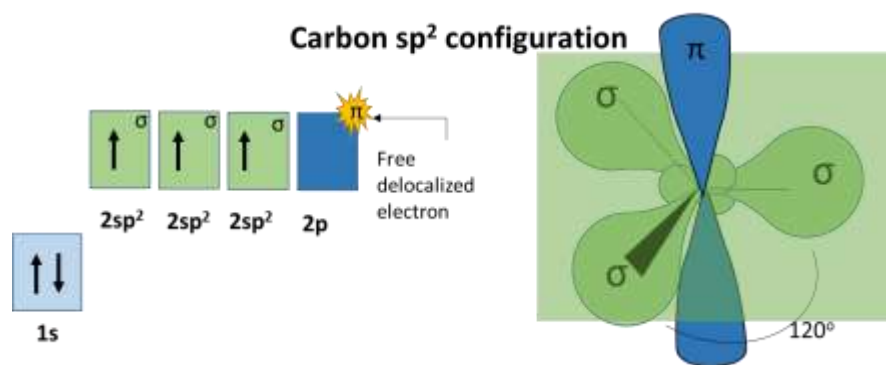


Figure 2.4 sp^2 configuration of Carbon

The formation of four sp^3 orbitals takes place when the 2s orbital hybridize with all the 2p orbitals. This hybridization is characterized by tetrahedral geometry. Diamond is based on this configuration and its properties are unique. Diamond is the hardest natural material on Earth, because of its strong σ bond among adjacent atoms[28], and has the smallest thermal expansion coefficient[29]. Because all the electrons are used in the σ bonds it does not have any free electron to travel, thus it is an electrical insulator.

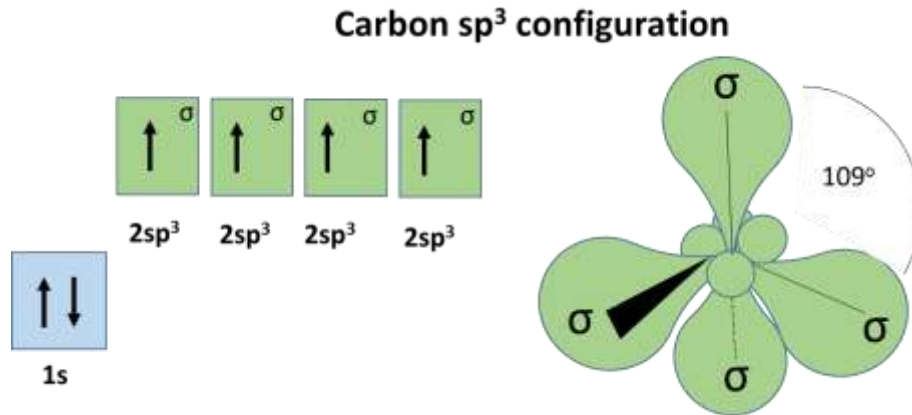


Figure 2.5 sp^3 configuration of carbon

This variety in chemical bonds makes carbon very unique among other elements in the periodic table. Consequently carbon can form up different atomic structures with amazing different properties. Some of the allotropes of carbon are fullerenes (buckyballs: C₆₀, C₅₄₀ and C₇₀) and carbon nanotubes presenting sp^2 configuration[30], Lonsdaleite (hexagonal diamond) is based on sp^3 configuration[31], and amorphous carbon (a-C) has a mixture of both sp^2 and sp^3 [32]. Amorphous carbon has different categories according to its structure and content of sp^2 and sp^3 bonding.

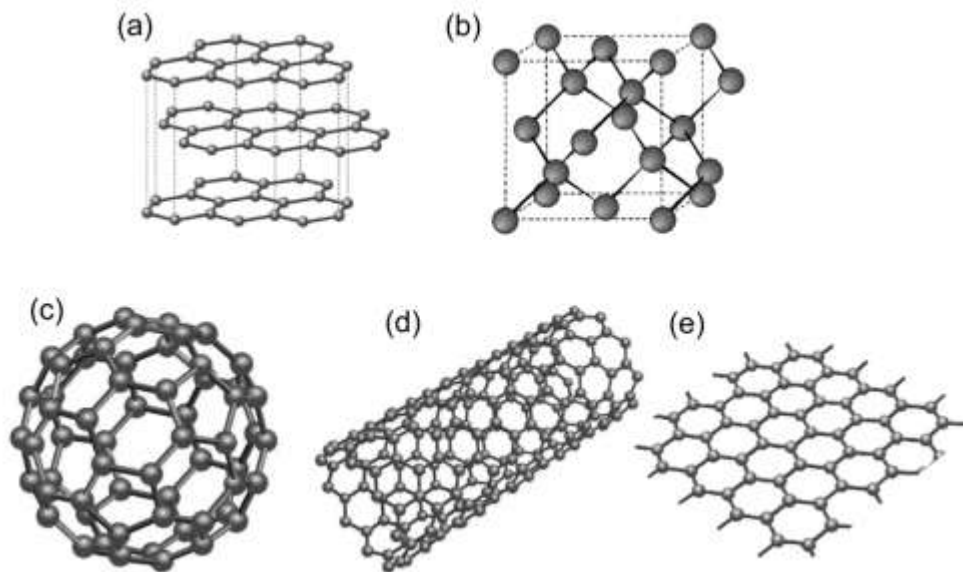


Figure 2.6 Different atomic structures of carbon: a) Graphite, b) Diamond, , c) C60 (Buckminsterfullerene), d) Single-wall carbon nanotube, and e) Graphene[33].

Amorphous carbon films are disordered networks constituted of a mixture of sp^2 and sp^3 hybridized bonds. a-C properties are strongly related to the ratio of sp^2 (graphite like) to sp^3 (diamond like) bonding configuration[34]. Among all the allotropes of carbon, just Diamond-Like Carbon is investigated in detail in the present thesis work.

2.3 Diamond Like Carbon Thin Films

When the amount of sp^3 bonds is considerable higher than the sp^2 bonds the chemical nature of the amorphous carbon is more inclined to diamond and metastable, it is called Diamond-like Carbon (DLC)[35].

2.3.1 Structure and Properties of DLC

DLC has been classified into two main categories of DLC: hydrogen-free DLC and hydrogenated DLC (a-C:H). Furthermore, when the sp^3 content is significantly high (90%), it is called tetrahedral amorphous carbon (ta-C)[36]. Fig. 2.7 illustrates different types of DLC.

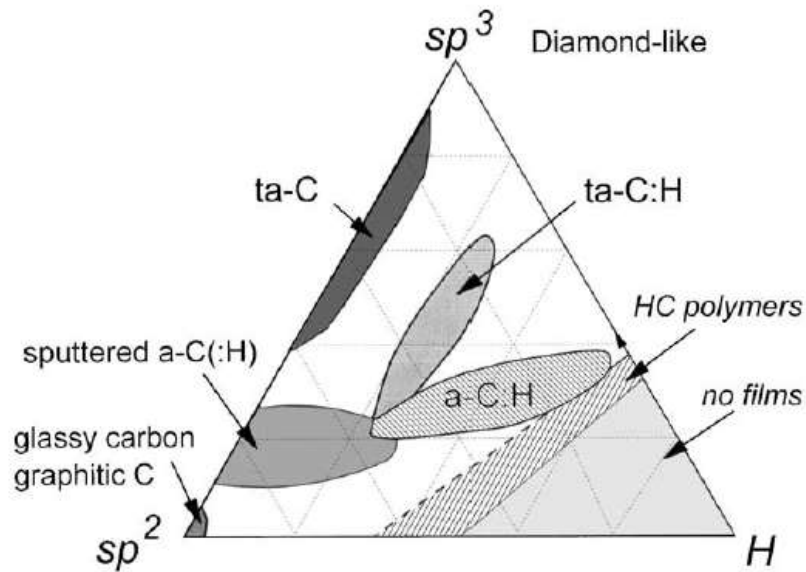


Figure 2.7 Ternary phase diagram of amorphous carbon with different sp^2 , sp^3 and H content [35]

It can be seen that graphitic and glassy carbon are located in the bottom left hand corner with the highest sp^2 content and free of hydrogen. DLC can be created with sputtering techniques by increasing the sp^3 content. Further escalation of sp^3 bonds will lead to tetrahedral amorphous carbon (ta-C) which is hydrogen free. By using hydrocarbons as precursors, the presence of hydrogen is inevitable. This hydrogen leads two regions in the middle of the diagram, tetrahedral hydrogenated carbon (ta-C:H) and hydrogenated amorphous carbon (a-C:H). If the hydrogen content is increased even more, the formation of polymers takes place. Finally, when the amount of hydrogen is higher than carbon (bottom right hand corner) there are no formation of films.

DLC has been investigated in the last four decades for its high hardness (approximately 80 GPa in ta-C and 50 GPa in ta-C:H), chemical inertness (to acids and alkalis), optical transparency (approximate refractive index of 2), high electrical resistivity, low coefficient of friction (0.05 to 0.2 on steel depending on test conditions), high wear resistance and biocompatibility. Fig. 2.8 simulates the structure of DLC with 10% of hydrogen, it can be seen sp^3 and sp^2 chemical bonds[37].

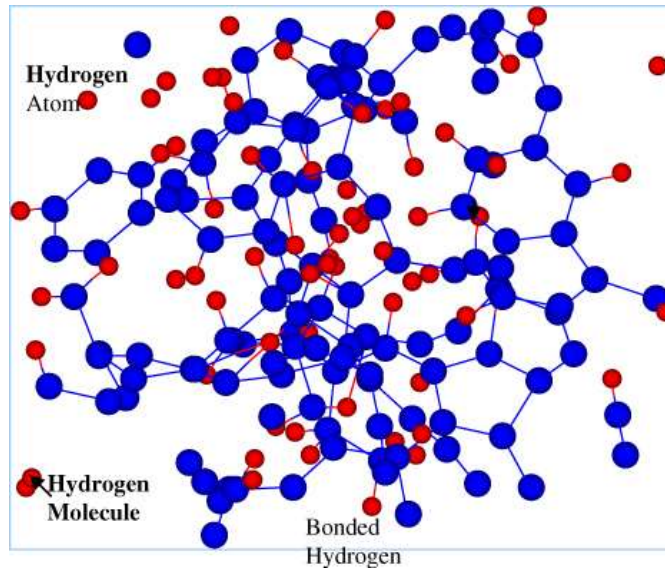


Figure 2. 8 Molecular dynamic simulation of atomic structure of a-C:H film [37].

2.3.2 DLC deposition techniques

DLC was synthesized for the first time by using ion beam deposition in 1971[38]. Since that time, different chemical vapor deposition (CVD) methods and physical vapor deposition (PVD) have been developed for both laboratory and industrial scale production. DLC can be manufactured by a wide variety of deposition techniques such as mass selected ion beam (MSIB), sputtering, filtered cathodic vacuum arc (FCVA), pulsed laser deposition (PLD), and plasma enhanced vapor deposition (PECVD).

MSIB has a well control over the ion species and its energy, a filtering out of neutral species and specific ions, and the ability to dope by switching the ion species. MSIB drawbacks are low deposition rate, high cost and voluminous apparatus size[39]. For industrial production sputtering is the most common method due to its adaptability to scale up and versatility to sputter different many materials[40]. Magnetron sputtering is usually applied to increase the deposition rate of the process, nevertheless this technique usually has low ratio of energetic ions to neutral species, and as a consequence the sp^3 content in the films is low. FCVA provides highly ionized plasma and high deposition rates, but the cathode spot is unstable and the insufficient filtering limits its

applications. PLD technique vaporizes many different materials including graphite to produce ta-C (high sp^3 content). This method is used mainly for research purposes since it is a laboratory scale technique, thus it has very limited industrial applications[41]. The most used method to deposit DLC at laboratory scale is PECVD, its description is given in Chapter 3.

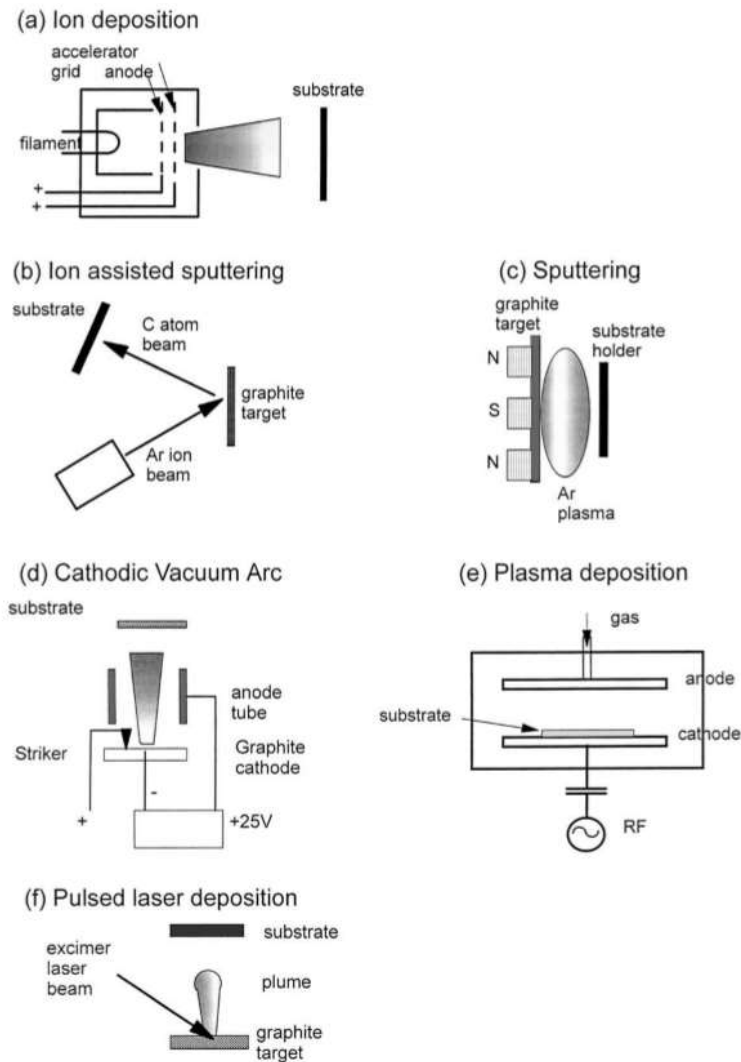


Figure 2.9 Diagrams of different DLC deposition techniques[35].

2.3.3 Deposition Mechanism

Bombarding the surface with energetic particles during the deposition is the key in the formation of high fraction of sp^3 C-C bonds, which provides the unique characteristics of metastable DLC[35,42]. Sub-plantation is the process in which energetic carbon ions are bombarded and implanted into atomic sites under the surface of the substrate. At the beginning of the process, the bombarded ions penetrate into the subsurface, then the incorporation of carbon and/or hydrogen induces local stress in the subsurface, followed of the creation of pure carbon level due to sputtering and dilution of target atoms, and the film continues growing with the formation of a new DLC layer from the successive bombardment[43].

The energy needed for carbon ions in order to penetrate the surface of the substrate is called penetration threshold, E_p . An ion particle needs a minimum energy in order to displace a surface atom from its original location and create a stable vacancy-interstitial pair. This minimum energy is called displacement threshold, E_d . Besides, the energy that keeps surface ions tightly together is known as binding energy, E_b . Thus, the total penetration threshold for a group of carbon ions with certain critical energy is defined by

$$E_p \sim E_d - E_b \quad (2.1)$$

If an ion does not possess enough energy to overcome the penetration threshold energy, it will not be able to infiltrate into the subsurface layer. This ion remains on the surface in its low energy sp^2 state. Only those ions with higher energy than E_p will be able to penetrate through the subsurface layer. Thus, this dynamic penetration of ions will increase the local density and energy, resulting in sp^3 bonding. While increasing the ion energy, ions will acquire enough energy to penetrate deeper into the surface, therefore, groups of ions are involved in different atomic effects such as displacement, thermalisation and relaxation[35]. This reduces the local atomic density and declines sp^3 bonding. Robertson [42] has reported an optimum ion energy value of 100 eV in order to form DLC thin film with high sp^3 fraction. In this way, ions have enough energy to penetrate the surface of the substrate and increase sp^3 bonding sites[44]. In others research work, it has reported 100 eV as the best approximate ion energy to achieve high sp^3 fractions regardless of the deposition technique[35,37].

2.3.3.1 Growth of Diamond-like carbon thin film

The growth mechanism of hydrogenated DLC is more complex than tetrahedral DLC. Although hydrogenated amorphous carbon formation follows the sub-plantation model, an important research effort is been focused to understand the growth mechanism and the role of hydrogen in the mechanism. When it comes to a-C:H deposition, different hydrocarbon sources can be utilized such as benzene, methane, ethane, propane and acetylene. The growth mechanism of hydrogenated DLC is divided into three major stages:

- 1.-Dissociation and ionization of precursor gases, plasma formation.
- 2.-Reaction of plasma with the growing film in the surface.
- 3.-Reaction in the subsurface layer of the film.

It is necessary to understand the physical process of sub-plantation, as well as the chemical process related to the interaction of ions, neutral species, radicals, and dehydrogenation for studying the complex growth model of a-C:H. Ions, neutral species, un-ionized precursor gas, mono and di-radicals, other unsaturated species such as C_2H_4 or C_2H_2 interact during the formation of plasma and deposition.

Growth rate is usually thermal independent nevertheless it can affect etching and consequently minimize growth. It has been suggested that the energetic surface might be quenched due to the thermal difference between the surface and cold underlying substrate. Then metastable DLC is frozen-in by this process, suggesting that a condensation mechanism is the reason why DLC cannot be obtained at temperatures higher than $400^\circ C$. Diamond-like carbon net has been proposed to arise due to the transitory high pressure and temperature spikes when the ion flux is impacting the surface[45].

The presence of hydrogen during the condensation of the film has been suggested to facilitate the formation of a carbonaceous amorphous structure with an average coordination number as close as a fully constrained network. Hydrogen can penetrate deeper through the sub

layers of the surface due to its small radical size. Since it has weak interaction with other atoms due to its chemical nature, it plays the role of a network terminator, decreasing the level of crosslinking and promoting the rearrangement of the network[46]. Hydrogen radicals can also form hydrogen molecules by bonding with other hydrogen atoms, leaving behind unsaturated dangling bonds on the subsurface. The overall process of a-C:H growth includes the physical process of sub-plantation, condensation of species in the subsurface, chemical interactions of different species in the plasma closed to the surface, and dehydrogenation-recombination. Figure 2.10 illustrates the growth model of a-C:H thin film suggested by Robertson[35].

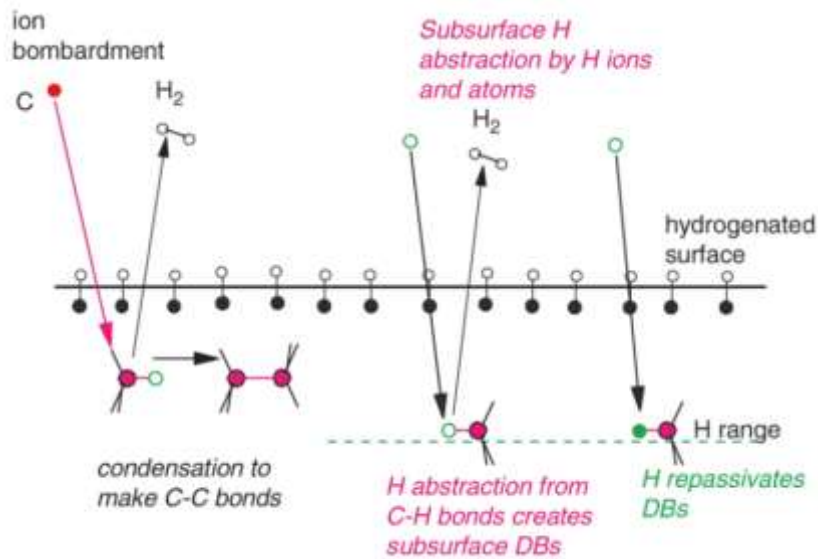


Figure 2.10 Growth mechanism of a-C:H[35].

2.3.4 Stresses in DLC

A significant amount of compressive stresses is introduced in the film due to the energetic ion bombardment. This stress increases in parallel with film thickness [47]. The introduction of stress in DLC is extremely adverse as it conducts to poor adhesion and consequent delamination of the coating. Good adhesion of DLC film is the basis of its successful industrial applications. Residual stress, σ , appeared in amorphous carbon films depends on three different classes according to its origin[48]:

- (a) Thermal stress (σ_{th}),
- (b) Intrinsic stress (σ_i) and
- (b) Extrinsic stress (σ_e).

The quantity of residual stresses can be calculated as follows:

$$\sigma = \sigma_{th} + \sigma_i + \sigma_e \quad (2.2)$$

2.3.4.1 Thermal Stress

The origin of this stress is due to significant differences between thermal expansion coefficients between the substrate and the film. It is important to consider the difference between the deposition temperature of the film and the temperature of the sample during determination of stress. Two main solutions have been investigated to minimize thermal stress in the films. The first approach is to deposit at room temperature, and the second one is to pre-deposit an interlayer with a thermal expansion coefficient between the film and the substrate[49].

2.3.4.2 Intrinsic Stress

Intrinsic stresses are created during deposition and are related to the morphology and microstructure of the films. Thus intrinsic stress is strongly depended on the deposition parameters. Intrinsic stresses in thin films can be classified into two types: tensile and compressive intrinsic stresses. Tensile intrinsic stresses are regularly originated by defects such as voids and vacancies in the films which are related to low energetic particles (0.1-1eV)[50]. Compressive stresses gradually rise to a certain value as the impact energy per atom increase (from 1eV to 25eV)[34,36]. Fig 2.11 shows the idealized behavior of intrinsic stress related to impact energy per atom [50].

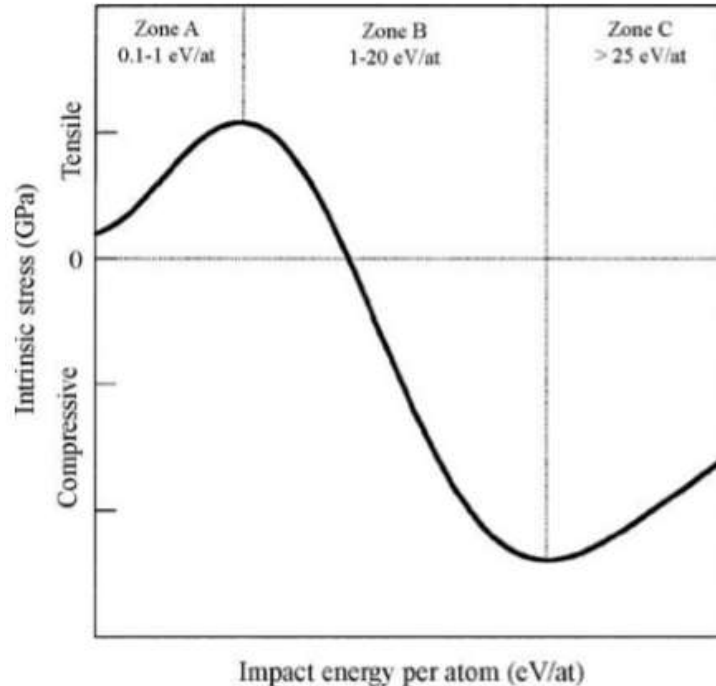


Figure 2.11 Idealized behavior of intrinsic stress with different impact energy per atom[50].

In order to explain the origin of compressive intrinsic stress in the coating a model was proposed known as knock-on process. In this model the implanted atoms under the surface through knock-on impacts create compressive intrinsic stresses. Then the energetic ions embedded into the subsurface transfer into a metastable location. On the other hand, energetic bombardment of other species provokes rapid local heating in certain zones while the energy is transmitted among surrounding atoms. Local heating energy or thermal spike supplies energy to the neighbor atoms to escape from their metastable position. After relaxation the subsurface started to cool down.

The balance between implantation and relaxation plays an important role in compressive intrinsic stress because is proportional to the ratio of ion flux (ϕ_i) to deposition rate (ϕ_d) [48], [50]. In order to minimize the compressive intrinsic stress in the films, two approaches can be chosen. One of them is to prepare films with low normalized fluxes (ϕ_i / ϕ_d), low energetic particle flow and high deposition rate. Alternatively film preparation with either high normalized fluxes (ϕ_i / ϕ_d), or low deposition rates with high ion fluxes can reduce compressive intrinsic stress[51].

2.3.4.3 Extrinsic Stress

Extrinsic stresses are generated by the interaction between the film and external factors. These external factors can be impurities of oxygen and/or hydrogen, grain surface energy reduction and reactions generating a new phase with a different molar volume. This changes leads to lattice deformation and film volume expansion, consequently stress formation.

2.4 Adhesion improvement of DLC on CoCrMo

As mentioned previously, CoCrMo implants become loose and release toxic ions due to the wear between moving surfaces and the corrosion in human fluids, which makes the implants fail[5]. In order to reduce the ion release and extend the life time of the implant, surface modification and coating have been investigated. Coatings can enhance surface characteristics and mechanical performance without altering the bulk properties of the implants and very promising to improve both the performance and the lifetime of the implants[6]. Diamond like Carbon (DLC) thin films have been attracted the most interest because of its extreme smoothness, low coefficient of friction, high hardness and excellent biocompatibility[37]. One of the key issues that limit the use of DLC is its poor adhesion to commonly used biomedical alloys like CoCrMo. The low adhesion has been attributed to the high compressive intrinsic stress of DLC due to the ion bombardment. Many approaches have been studied in order to minimize the stress[39–43]. Doping an element that reduces the stress is one of the main approaches investigated and positive results have been achieved. Hence, doping of DLC will be discussed in the following sections.

2.5 Doping of DLC

Doping is the incorporation of elements into films with different bonding states in order to modify the structure and improve specific properties. Some elements can be doped into DLC, creating more flexible bonds in the coating, and consequently reducing compressive stresses[51]. It has been reported that doping different elements into DLC can minimize compressive stresses

without sacrificing its admirable properties[37]. Nevertheless it has been presented that hardness can be reduced or increased even with the same doped element but with different deposition techniques[44–46].

One of the advantages of DLC is that due to its amorphous structure is possible to incorporate different elements in the carbonaceous net. As a result of doping DLC, different chemical bonding combinations leads to magnified properties for specific applications. It is crucial to consider the introduced amount, dispersion, and chemical nature of dopants during deposition in order to achieve the preferable properties and preserving the diamond-like characteristics in the film. As mentioned previously, according to the desirable property, different elements can be used to doped DLC. Some dopants can be light elements such as Boron, Silicon, Nitrogen, and Oxygen, also metals can be doped such as Nickel, Titanium, Tungsten, Silver, and Cobalt. Even it is possible to mix elements and dope them at the same time. Figure 2.12 illustrates different dopants and their effect on improving DLC properties[37].

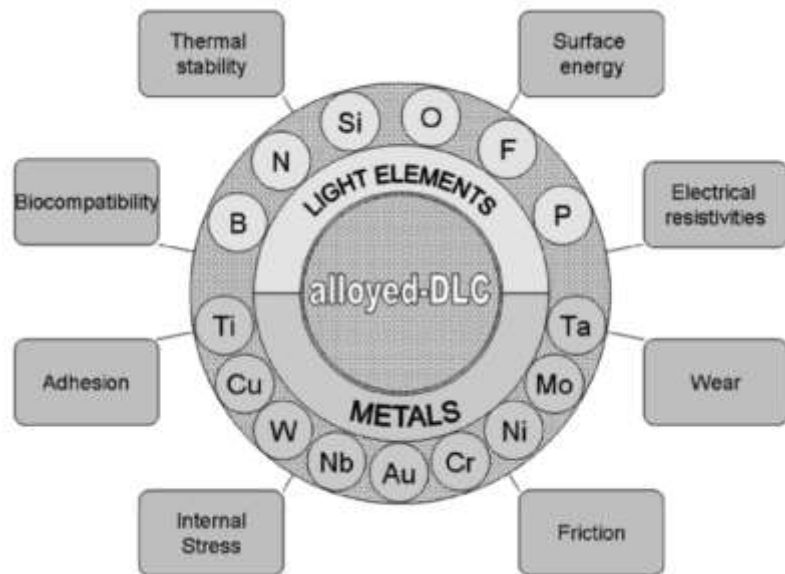


Figure 2.12 Scheme of known DLC dopants to improve particular properties[37].

2.6 Nitrogen doped DLC

Among other elements, Nitrogen is one of the most studied elements to dope DLC due to its diverse applications which it has been attracted research attention in past decades[55]. The first carbon nitride films were synthesized by Cohen and his colleagues during 1990's[56]. They anticipated that crystalline β - C_3N_4 structure could be harder than diamond. Despite of intense research effort, successful synthesis of ultra-hard β - C_3N_4 has not yet been concluded, nevertheless nitrogenated DLC films became popular since then. It is possible to form sp^2 and/or sp^3 sites by incorporating Nitrogen in DLC films because Nitrogen can form many bonding configurations. Nevertheless when Nitrogen does not dope DLC structure; it can form non-doping species such as Pyridine, pyrrole, and nitrile as shown in Fig. 2.13.

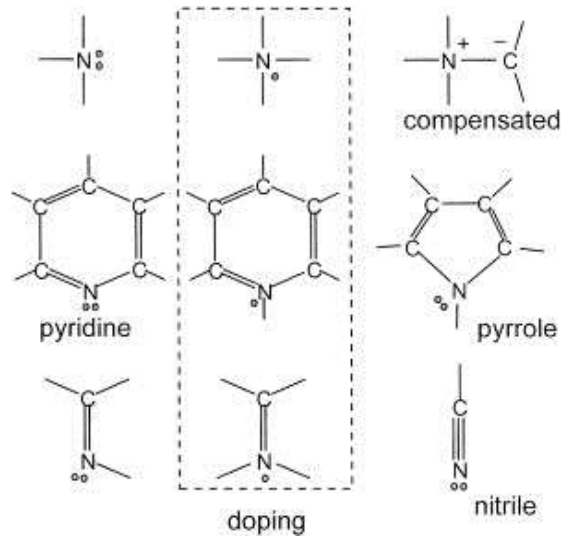


Figure 2.13 Different Nitrogen-Carbon configurations[35].

When a certain amount of nitrogen is doped into amorphous carbon, pentagonal rings can be formed and cross-linking between graphitic planes can be promoted as shown in Fig. 2.14. Due to the strong three-dimensional covalently bonded network, films with high elasticity and enhanced toughness could be synthesized[57].

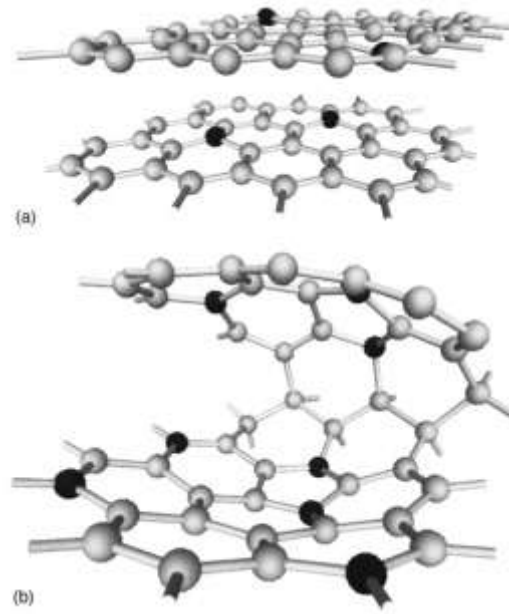


Figure 2. 14 Cross-linking of graphitic structures with formation of pentagons by increasing nitrogen concentration in the films from a) 5% to b) ~15%[57].

Less than 50 vol% of Nitrogen doping could form of sp^2 configuration due to possible formation of isocyanate ($N=C=O$) or nitrile ($C\equiv N$) groups, nitrile triple bond may terminate a chain[58]. Nitrogenated amorphous carbon with low sp^3 content would be softer and with better tribological properties than undoped DLC[50–52]. Under the appropriate deposition conditions and nitrogen content, other species with sp^2 character can be present such as $C=C$ and $C=N$ [62]. Increasing the sp^2 content by Nitrogen doping, decreases the average coordination number of carbon and consequently reduces the internal stress[58]. Thus Nitrogen doping is a potential approach to reduce residual stress and improve DLC adhesion[44-45]. Although many studies have been carried out on nitrogenated DLC due to its excellent mechanical properties and biocompatibility, limited studies have been reported using Plasma Enhanced Chemical Vapor Deposition on CoCrMo substrate. Therefore, by changing the content of Nitrogen in N-DLC would be beneficial to understand the relation between structure and properties and adhesion on CoCrMo.

2.6 Structural characterization of DLC thin films

2.6.1 Raman spectroscopy

Raman spectroscopy is a non-destructive structural characterization technique based on the inelastic scattering of light by a specific matter[63]. Raman scattering comes from incident radiation inducing transitions in the atoms or molecules that create the scattering medium. These transitions can be rotational, vibrational, electronic, or their combination [64]. In a Raman test, the sample is irradiated with monochromatic radiation. The inelastically scattered light is collected and dispersed. The resulting Raman spectrum plots the intensity of the inelastically scattered light as a function of the shift in wavenumber of the radiation. The practical suitability of Raman spectroscopy consists in the fact that the Raman spectrum serves as a fingerprint of the scattering material.

The information obtained from Raman spectroscopy includes the intensity of interatomic and intermolecular bonds, the mechanical strain existing in a solid, the composition of multicomponent matter, the crystallinity degree of a solid, and the effects of pressure and temperature on phase transformations. An important advantage of Raman spectroscopy (compared to x-ray diffraction) is the ability to provide detailed structural information of amorphous materials such as DLC[65]. Diamond has a single Raman active mode at 1332 cm^{-1} . Single crystal graphite has a single Raman active mode at 1580 cm^{-1} known as “G” for “graphite”. Disorder graphite has a second mode approximately at 1350 cm^{-1} called “D” for “disorder”[59, 60].

These two G and D modes of graphite are dominated by scattering of sp^2 sites. G mode is related to stretching vibration of sp^2 bonds such as C=C chains or aromatic rings. De-convolution of D and G peaks provides detailed information about D and G peaks, Breit-Wigner-Fano (BWF) is extensively used to fit G peak and Lorentzian to fit D peak. Therefore, it is possible to study the structural information of DLC by using Raman spectroscopy[68]. Figure 2.15 shows different Raman spectra of different carbon structures [35].

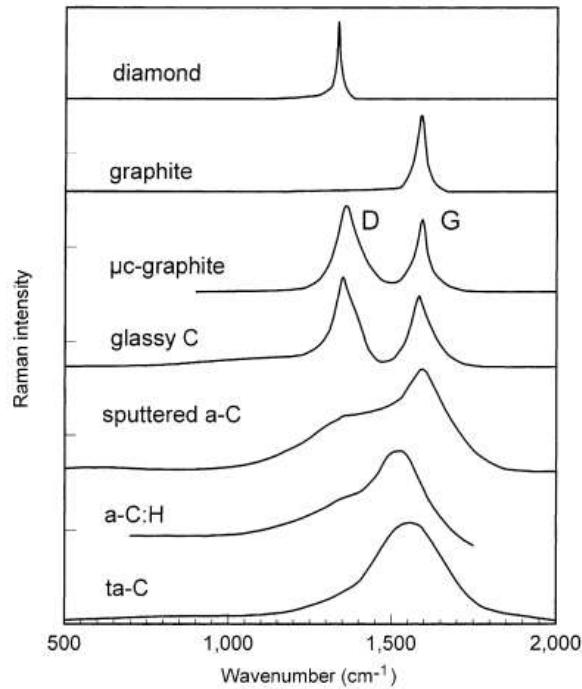


Figure 2.15 Raman spectra comparison of diamond and amorphous carbon structures [35].

2.6.3 X-ray photoelectron spectroscopy

X-ray photoelectron spectroscopy (XPS) uses X-rays of a characteristic wavelength to excite electrons from atomic orbitals. The photoelectrons emitted from the material are collected as a function of their kinetic energy. The number of photoelectrons measured in a certain time interval is plotted versus kinetic energy. Thus XPS spectrum consists in electron counts (number per second) versus electron kinetic energy (eV). Figure 2.16 illustrates the process of photoemission[69].

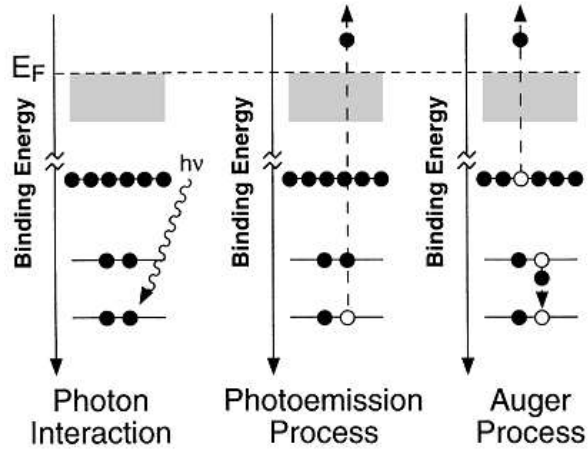


Figure 2.16 Schematics of the excitation, photoemission and Auger processes [69].

Conservation of energy takes place in the photon absorption process. The kinetic energy (E_k) is equal to the incident photon energy ($h\nu$) minus the initial binding energy (electronic ground states) of the electron (E_B).

$$E_k = h\nu - E_B \quad (2.3)$$

Since initial energy of X-ray ($h\nu$) and kinetic energy of released electrons (E_k) are known, the graph can be plotted in terms of binding energy (E_B) which is characteristic for each element. The positions of the peaks identify the chemical bonds in the material. Peak areas are proportional to the number of orbitals in the analysis volume and are used to quantify elemental composition. The positions and shapes of the peaks in an XPS spectrum can also be analyzed in greater detail to determine the chemical state of the constituent elements in the material, including oxidation state, partial charge, and hybridization.

XPS is a surface sensitive technique. The nominal analysis depth is on the range of 1 to 10 nm (10 to 100 monolayers). For that reason this technique is not appropriate for bulk characterization. All elements with atomic number greater than three can be detected. The main limitation of XPS is the need for ultrahigh vacuum in the chamber during the test. Thus materials with low vapor pressure ($<10^{-8}$ mbar) at room temperature cannot be analyzed. Some polymeric materials can also degrade under the x-ray flux. XPS is a widely used characterization technique for a-C:H [22,44,51,64–67]. In DCL XPS spectra is dominated by Carbon states because the cross-section of Hydrogen states is weak [35].

2.7 Mechanical characterization

2.7.1 Nanoindentation

In order to measure a reliable bulk hardness value in a film, the film thickness should be numerous times greater (at least ten times) than the penetration depth of the indenter [74]. In this way the measured value of hardness will not be influenced by the substrate deformation below the film. Usually this criterion is difficult to accomplish using standard microhardness technique since many wear-resistant materials are often deposited in the range of 1–5 μm thick such as DLC. Even when the indentation is kept within the 10% of film thickness, another deviation from the real hardness value is to ignore the effects of indentation size. Many ceramic materials and metals can show increased hardness values when the load is lower than 0.1 kgf[75] Some high hardness values cited in the literature might be influenced by the indentation size effect (ISE).

There are two methods to measure the hardness of a coating: direct coating hardness measurement for thick coatings, and modeling the hardness behavior of thin films for thin coatings. For thick coatings, measuring hardness in a range of loads allows to determine directly both the hardness value at a fixed indentation size (usually 10 μm), and the ISE index. On the other hand, for thin films a modeling approach must be used to determine the real coating hardness and ISE index due to the substrate effect on the measurement[76]. Although direct coating hardness measurement has been used habitually for many years, may not be possible to measure accurately the properties of a thin film independent of the substrate, unless the coating is very thick by using conventional testing equipment. Consequently, specialized instruments have been developed and have become commercially available, they are known as ultra-low load microhardness testers or nanoindenters.

A common characteristic among nanoindenters is the continuous monitoring of the load and displacement as the indentation is penetrating the film. The projected area of the indentation needs to be determined from the load/displacement data, in order to calculate the hardness from such depth sensing indentation test. Elastic and plastic deformations are included in the measured displacements, thus it is necessary to eliminate the elastic contribution in order to calculate just

the plastic depth from which the area can be determined using the geometry of the indenter. Fig.2.17 shows a characteristic hardness plot for tetrahedral hydrogenated DLC[77].

A tangent line is marked to the unloading curve from the maximum load point to the zero. The Young's modulus is related to the slope of this tangent line. The hardness H can be calculated as

$$H=0.0378(L_{max}/h_p^2) \quad (2.4)$$

where h_p is the deplastic deformation, L_{max} corresponds to the maximum load, thus the elastic deformation is the difference between the maximum indent h_{max} and h_p . Then, the Young's modulus E can be expressed as

$$E = 0.179 \frac{(1-\nu^2)L_{max}}{(h_{max}-h_p)h_p} \quad (2.5)$$

The accuracy strongly depends on the indentation depth and the thickness of the film. Another important consideration is that nano-hardness testers can be very sensible to vibration and sample roughness.

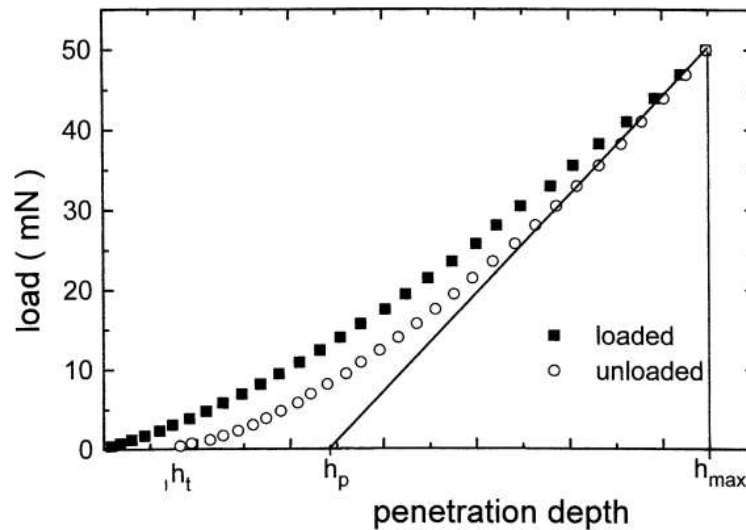


Figure 2.17 Typical loading unloading graph for ta-C:H Nano-hardness test[77]

2.7.2 Rockwell C indentation

Some of the most common direct methods to analyze adhesion are tensile (pull) test, peel test, scratch and tape test. Nevertheless these techniques do not provide information about the interface toughness, and some of them are design for low adhesion coatings like paint. Rockwell C indentation tester is a low cost qualitative technique commonly used for indirect adhesion measurement of diamond-like carbon coatings[72–75]. A load of 1471 N is perpendicularly applied to the film with a diamond “C” indenter, and the area around the indent is evaluated under microscope after indentation. The damage degree around the circular perimeter of indentation is compared with a well-established adhesion quality guideline known as VDI guidelines 3198[81]. Figure 2.18 shows the quality of adhesion strength from HF1 to HF6 stages[82]. From HF1 to HF4 stages are considered as strong adhesion quality based on the VDI guidelines, while HF5 and HF6 correspond to insufficient adhesion quality. In the present study, Rockwell C testing was used to compare adhesion strength of different DLC samples by using a load of 1497N.

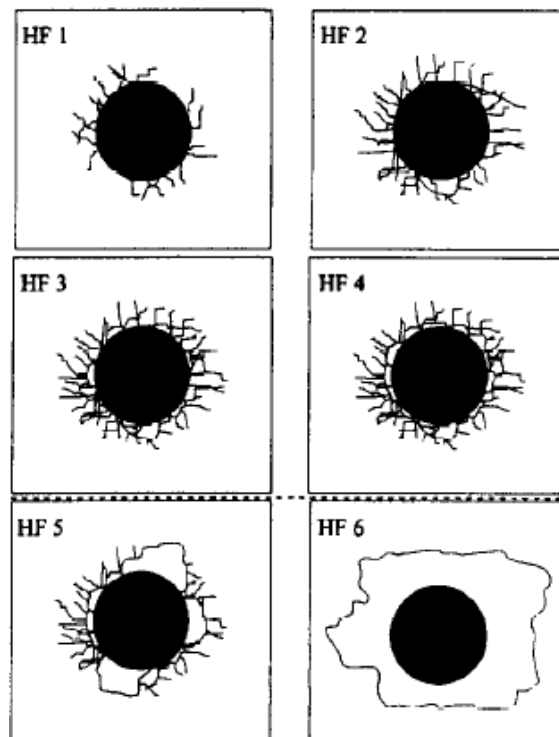


Figure 2.18 Schematics of different adhesion stages according to VDI 3891 guideline[82].

2.7.3 Scratch test

In scratch test a stylus draws a line over the sample surface under a stepwise or continuous mode while the normal force increases until the coating detaches. It is necessary to determine the critical load (L_c) associated to the adhesion of the coating during the test. L_c is the load at which the coating is removed in a regular way along the whole channel length. Delamination of the film can be detected in different individual or simultaneous ways: (a) optical or scanning electron microscopy, (b) acoustic emission, and (c) friction force measurement. The sensitivity of this method is relatively higher if the frictional force measurement is considered. Scratch test is widely used as a quantitative adhesion measurement for thin carbon hard coatings[83]. Figure 2.19 shows a typical scratch test [84].

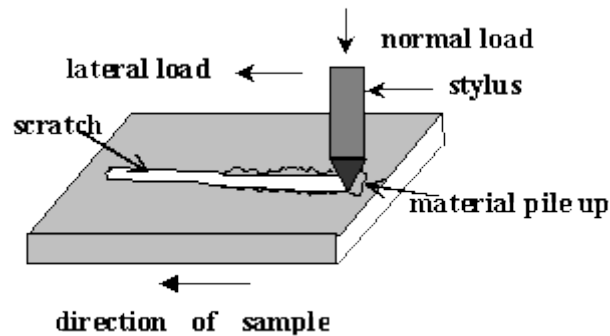


Figure 2.19 Schematic image of scratch test[84]

2.7.4 Friction and Wear resistance

Friction is measured by the movement of surfaces in contact with each other while a load is applied over them. Static friction is measured during the application of the load, then the surfaces start to move and dynamic friction is analyzed. Friction strongly depends on the conditions of the test, in other words, it is not a fundamental property of a material. Friction measurements are sensitive to surface chemistry, hardness, and morphology.

The coefficient of friction describes the ratio of the moving force between two surfaces and the applied load on them. Another extrinsic property of a material is wear. Wear is the deformation and loss of a material in dynamic contact with another material. Wear of a film can

be expressed by weight loss measurement, and/or wear tracks analysis. Wear is also sensitive to the conditions of the test such as temperature, humidity, materials in contact, etc. Thus most wear tests are designed according to the final application requirements. In the present work, friction and wear were measured under ball-on-disk configuration. Figure 2.20 shows a schematic of a ball-on-disk configuration.

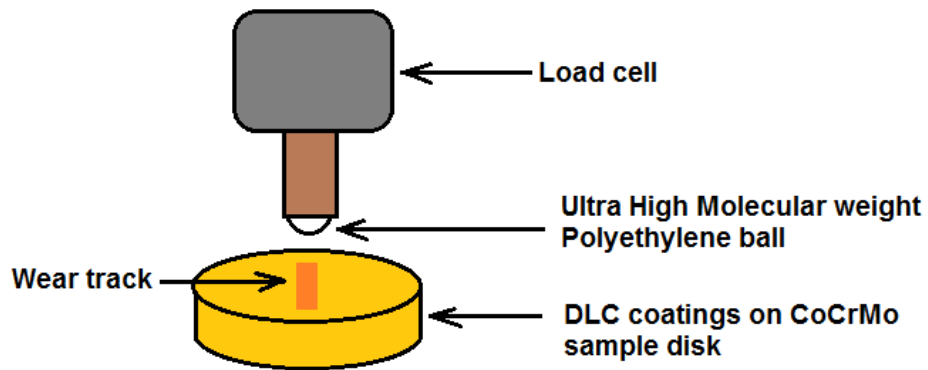


Figure 2.20 Schematic image of a Ball-on-disk configuration.

CHAPTER 3 – MATERIALS AND METHODS

3.1 Thin Film Deposition

In the present research, microwave plasma enhanced chemical vapor deposition (MPCVD) was used to grow microdiamond particles before DLC and N-DLC films were deposited by plasma enhanced chemical vapor Deposition (PECVD). After deposition, structural characterization was performed with Raman spectroscopy and X-ray photoelectron spectroscopy (XPS). Surface morphology was observed by an optical profilometer. Mechanical properties were measured by nano-indentation tests by using universal testing machine (UTM), and tribological behavior was evaluated with a ball-on-disk configuration in the UTM. The details of the procedures are explained in the following sections.

3.1.1 MPCVD System

Microwave Plasma Chemical Vapor Deposition system (model: MWPECVD 1250UOS) manufactured by Plasmionique Inc. was used to grow microdiamond particles on CoCrMo alloy prior DLC deposition. The system consists of a ASTEX-type 2.45 GHz microwave source, a stainless steel vacuum chamber, a pumping system, a gas flow system and a manual control system as represented in Figure 3.1. The microwave source can be tuned to provide maximum power up to 1.2 kW. The vacuum chamber contains a substrate stage that can be vertically adjusted to minimize microwave power reflection. The elevated temperature required for diamond deposition is reached through plasma heating and it is controlled by the microwave power. A mixture of hydrogen and methane (1 vol. %) with a total flow rate of 100 sccm were used as precursors, the flow rate was controlled by a multi-channel flow meter.

CoCrMo samples were prepared by grounding with silicon carbide paper (800 grit size) and fine polished with diamond slurry of 9 μm , 3 μm , and 1 μm , sequentially. Then the CoCrMo samples were seeded ultrasonically in a nanodiamond particle suspension manufactured by Mark

V Laboratory for 40 min to improve the nucleation sites of diamond. The microwave power used was 800 W and the growth was for 1 hour.



Figure 3.1 Photograph of MPCVD System

3.1.2 Chemical Vapor Deposition System

DLC deposition was carried out on both CoCrMo alloy samples and silicon (100) wafers using plasma enhanced Chemical vapor deposition (PECVD) reactor made by Plasmaionique Inc., located in room 0C17, Engineering building. The system consists of a high vacuum chamber, a pumping system composed of a mechanical and turbo pump, a rotating substrate holder, and two inductively couple plasma sources as shown schematically in Figure 3.2.

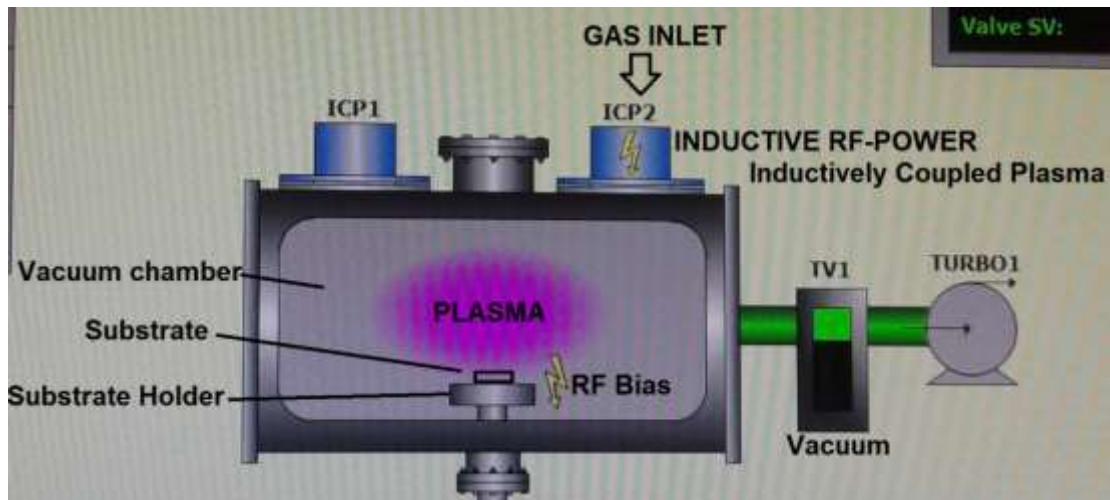


Figure 3.2 Schematic of PECVD

The PECVD technique is one of the three methods available in the hybrid system; the other two are physical vapor deposition (PVD) and pulsed laser deposition (PLD) mentioned previously in chapter 2. PECVD combines physical and chemical process. There are two types of CVD reactions, homogeneous and heterogeneous. Homogeneous reactions take place in the gas phase, thus particles can form before deposition. This leads to low density films, poor adhesion and defects in the films. Homogeneous reactions usually lead to low deposition rates because they consume reactants. On the other hand, heterogeneous reactions happen in the surface of the substrate. These reactions are favored in the PECVD system and culminate in the formation of the desired film. The main advantage of PECVD is that films can be deposited at low temperatures where some reactions would not take place in thermal CVD. The low temperature during deposition is beneficial for substrates with low melting point or for materials with a big difference between thermal expansion coefficients such as CoCrMo alloy and DLC, reducing thermal stress and consequently better adhesion. Figure 3.3 shows a picture of the PECVD reactor used for DLC and NDLC deposition.

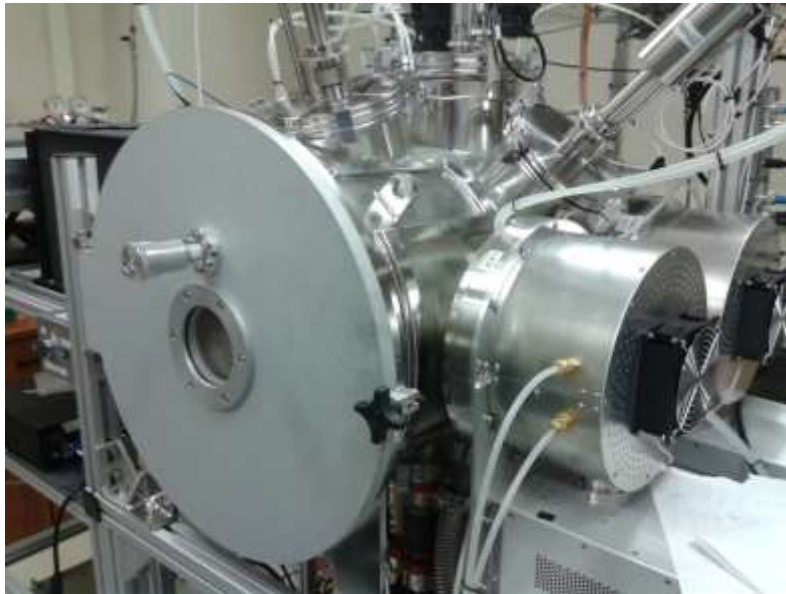


Figure 3.3 Photograph of plasma enhanced chemical vapor deposition system

In the present thesis work, a mixture of methane (CH_4), argon (Ar) and nitrogen (N_2) were used as precursors. CH_4 and Ar gas flow rates were kept at 40 sccm and 60 sccm respectively for pure DLC films while four different nitrogen flow rates were used (4 sccm, 8 sccm, 12 sccm and 16 sccm) to synthesize films with different concentration of nitrogen. After changing one variable at a time, the best RF power used was 150 watts with a bias of 60 V, and they were kept constant for all the samples in order to maintain the same ion energy of all the depositions.

The substrate temperature was set at room temperature nevertheless despite of the integrated cooling system in the chamber, the energetic ion bombardment increased slightly the substrate temperature at 30°C which was observed consistently for all the depositions. Although the recommendable substrate rotation speed by the manufacturing company of the equipment is 5 rpm, it was found that the substrate rotation at 3 rpm provided a better coverage of the whole sample and was set constant for all the depositions. The working pressure was maintained at 10 mTorr which was the best working pressure found for DLC deposition with the set values of the other variables. The deposition time was set for 2 hours, generating a film thickness between 600 and 650 nanometers. Each sample was repeated 4 times in order to observe consistency in the deposition rate, have repeatability and enough samples for structural, mechanical and tribological characterization. The detailed deposition parameters are summarized in Table 3.1.

Table 3.1 Deposition parameters employed in DLC and NDLC films

Sample	Gas flow rate (sccm)			Working Pressure (x 10 ⁻⁶ torr)	Temperature (°C)	Power (watts)	Bias (Voltage)	Thickness (µm)
	N ₂	CH ₄	Ar					
DLC	0	40	60	10	30	150	60	0.61
D-NDLC-1	4	40	60	10	30	150	60	0.62
D-NDLC-2	8	40	60	10	29	150	60	0.61
D-NDLC-3	12	40	60	9	29	150	60	0.63
D-NDLC-4	16	40	60	10	33	150	60	0.61

3.2 Structural Characterization

A Reinshaw 2000 Raman spectroscope was used to determine the type of carbon structure obtained and ration sp² (graphite like) to sp³ (diamond like) bonding configuration in the coatings. The equipment is located at Saskatchewan Structural Science Center (SSSC), University of Saskatchewan. The measurements were taken at 514.5 nm wavelength with Ar ion laser in a spot size of 1.5 µm approximately. Internal calibration with silicon standard was performed before every test. Three different spots were analyzed for each samples with the exposure time of 40s, accumulation of data was kept at 4 times to reduce noise in the lectures and cosmic rays removal mode was active in order to avoid suspicious peaks from cosmic rays. The background of the spectra was removed for all the samples in order to facilitate their analysis and comparison. Figure 3.4 shows the Raman instrument employed in the present work.



Figure 3.4 Reinshaw 2000 Raman spectroscope

X-Ray photoelectron spectroscopy (XPS) measurements were performed at the Canadian Light source (CLS) with a monochromatized Al K (alpha) X-ray source to study the composition and bonding states of the deposited films. The measurements were carried out with the assistance and supervision of Dr. Ronny Saturto CLS scientist. XPS analysis requires an ultra-high vacuum in the range of $\times 10^{-9}$ Torr which is reached in a small chamber. Consequently, sample dimensions were 4 mm^2 . By scanning each sample 5 times the noise was minimized and reproducibility was confirmed. Casa XPS software version 2.3.18 was employed to analyze the obtained data.

3.3 Surface Morphology

Zygo NewView 8000 optical profilometer located in room OC19 at Engineering building was used to study the surface topography and film thickness of the films. One of the intrinsic properties of diamond is optical transparency, high sp^3 DLC inherit this property. For that reason a refractive index of 2 was set in the equipment in order to collect the data. The Joel JSM-6010LV scanning electron microscope (SEM) located in room 2C25 at Engineering building was used to observe the surface morphology after the Rockwell C indentations and wear testing.

This equipment was also employed to observe the distribution of microdiamond particles on cobalt alloy substrates prior deposition of DLC films. Figures 3.5 and 3.6 show the optical profilometer and the SEM respectively used in this study.



Figure 3.5 Picture of Zygo NewView Optical profilometer

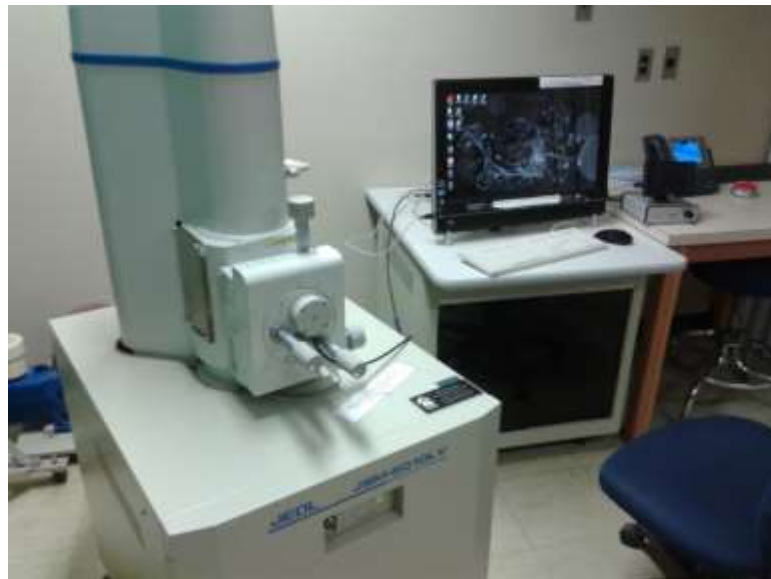


Figure 3.6 Picture of JOEL JSM 6010 LV Scanning electron microscopy

3.4 Mechanical testing

Hardness and Young modulus were measured by nano-indentation tests using a Universal Mechanical Tester (UMT) located in Room 1B22, Engineering Building. A 100 nm Berkovich indenter tip was placed perpendicular to the sample surface and entered into the sample by increasing the load to the desired value (loading). The indenter is left in this maximum load for 60 seconds, in order to minimize any effect on the measurement due to possible creep of the material[80–82]. The load then gradually decline to the origin where total or partial relaxation of the coating has occurred (unloading).

In the present work, a matrix of 3 x 3 spots was set for each sample to ensure the reproducibility of the hardness data. After a scan test with variable loads from 2mN to 100mN, the load of 5mN was chosen because it guaranteed the indentation depth was less than 10% of the coating thickness to avoid any effect from the substrate as explained in section 2.7.1. Load and indentation depth data were constantly collected to calculate the film hardness and Young's modulus of the films by the software based on Oliver and Pharr method[88]. Figure 3.7 displays the picture of nano-indentation system.

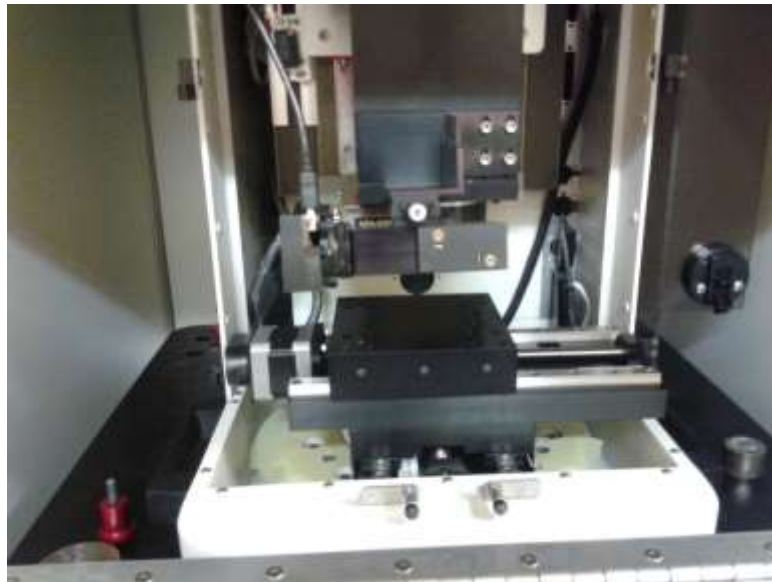


Figure 3.7 Picture of Universal Mechanical Tester for nano-indentation investigation

Rockwell C indentation was performed to evaluate qualitatively the adhesion strength of the coatings by applying a repetitive standard load of 1497 N. Three different regions were indented for each sample and then observed using the SEM for their analysis. According to VDI guideline a film with sufficient adhesion should present less spallation, damage and cracks around the circular imprint. Figure 3.8 shows the image of the Rockwell C equipment used located in room 2C25, Engineering building.



Figure 3.8 Rockwell C indenter

3.5 Tribological Characterization

Friction and wear analysis were effectuated using another Universal Testing Machine (UTM) placed in room 1B22, Engineering building. A ball-on-disk configuration was set by using Ultra High Molecular Weight Polyethylene (UHMWPE) balls immerse in distilled water at room temperature in contact with DLC and NDLC coatings (disk samples). A constant load of 10N was used for all the samples which is higher than other researches have been used at 1N[72] and 2N[89–91], nevertheless the ISO 14242 Implants for surgery- wear of total-hip joint prostheses[92], recommends a force range from 0.3kN to 3kN in a cyclic loading under simulated

body fluid at 37°C. The parameters in the present research work were set based on the capabilities of the equipment. A linear reciprocating motion was set, and the displacement length was constant at 2.5 mm. 10000 cycles were carried out for all the samples. Figure 3.9 shows the UTM with a configuration ball-on-disk for the DLC samples.



Figure 3.9 UTM (left) and Ball-on-disk configuration for friction and wear tests (right).

CHAPTER 4 – RESULTS AND DISCUSSION

The present chapter is divided into two parts. Section 4.1 focuses on the comparison of adhesion among pure DLC, microdiamond particles and DLC, and microdiamond particles and nitrogenated DLC films. It emphasizes the effect of pre-deposited microdiamond particles and nitrogen doping on the adhesion of DLC. Section 4.2 describes the adhesion and tribological behavior of the nitrogen doped DLC with different nitrogen contents.

4.1 Adhesion Enhancement of DLC on CoCrMo Alloy by Microdiamond particles and Nitrogen Incorporation.

In this section it is presented how micro-diamond particles and nitrogen doping into DLC improved adhesion of the films on CoCrMo and their effects in surface morphology and mechanical properties. Further chemical analysis of NDLC coatings by X-Ray Photoelectron Spectroscopy is presented in section 4.2.

4.1.1 Chemical Characterization

4.1.1.1 Raman Spectra and SEM of Diamond micro-particles on CoCrMo

Raman spectrum of CoCrMo samples after diamond deposition is shown in Figure 4.1. The peak at 1332 cm^{-1} indicates the presence of diamond microparticles on the surface while the peak at 1600 cm^{-1} coexists, indicating the formation of graphitic carbon. Figure 4.2 illustrates a SEM image of the samples after diamond deposition and it shows microdiamond particles uniformly grown on the CoCrMo substrate.

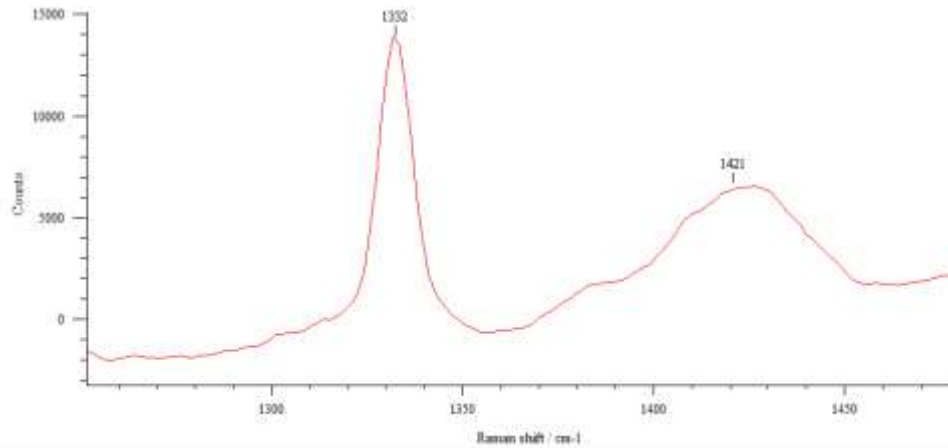


Figure 4.1 Raman spectra of micro-diamond particles on CoCrMo alloy

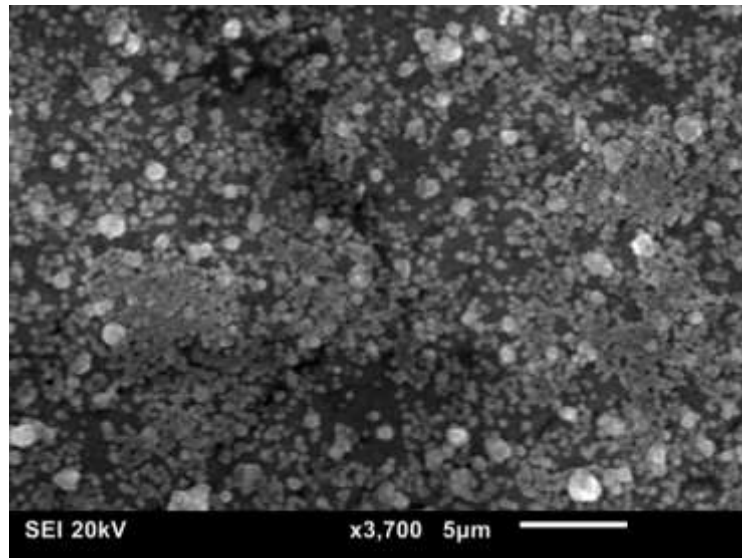


Figure 4.2 SEM of deposited micro-diamond particles on CoCrMo alloy

4.1.1.2 Raman Spectra of DLC and N-DLC

The Raman spectra obtained from deposited DLC and NDLC on silicon wafers are shown in Figure 4.3. The broad curves confirm the characteristic amorphous nature of the deposited films. Disordered D peak at around 1310 cm^{-1} and the graphitic G peak at around 1530 cm^{-1} are typical peaks of DLC present in all the spectra. The ratio of their intensities (I_D/I_G) provides an estimate of the sp^2/sp^3 bonding ratio in DLC structure. If the ratio is high, the sp^2 bonding percentage

increases in the film. DLC and NDLC deposited on silicon wafers show I_D/I_G ratios of 0.51 and 0.89, respectively.

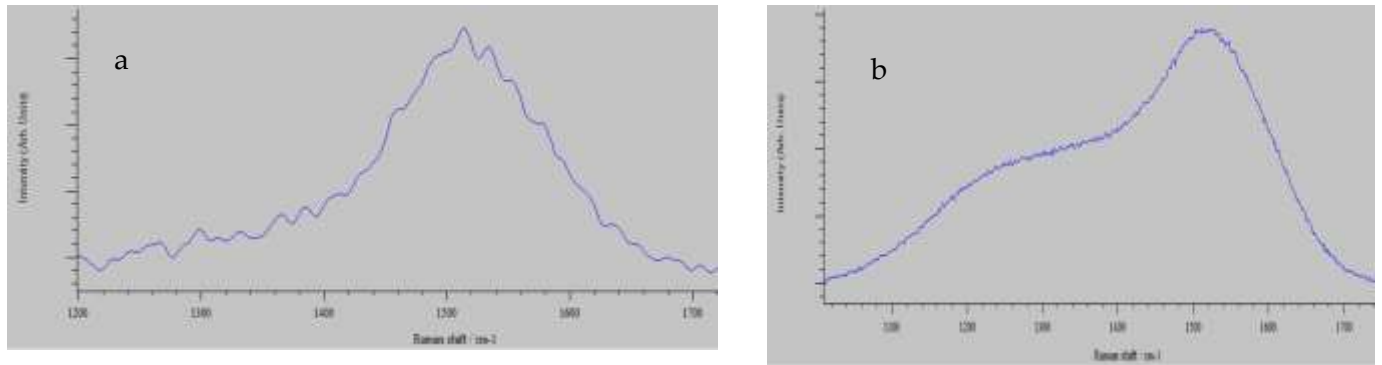


Figure 4.3 Raman Spectra of (a) DLC and (b) NDLC on silicon

Figure 4.4 shows the Raman spectra of DLC and N-DLC with the incorporation of diamond particles on CoCrMo specimens. It can be seen that microdiamond incorporation notably increases the intensity of D peak while I_D/I_G ratio is observed to be 0.67 and 1.38 for DLC and NDLC, respectively. This suggests that N doping also promotes sp^2 bonding in DLC coatings.

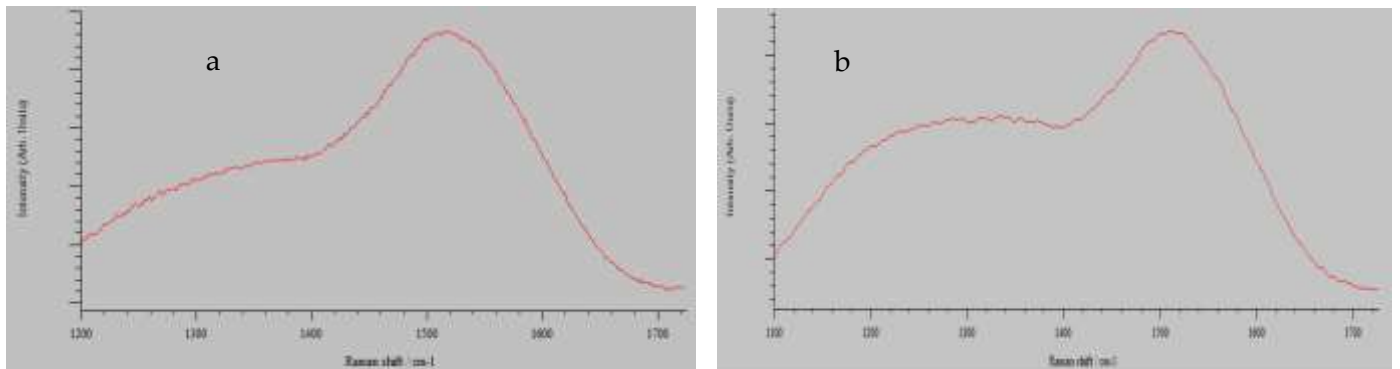


Figure 4.4 Raman Spectra of (a) D/DLC and (b) D/NDLC on CoCrMo alloy

4.1.2 Surface Morphology

Surface morphology of DLC films on CoCrMo samples with and without diamond incorporation was observed by SEM images. Figure 4.5 (a) shows spallation of DLC deposited directly on CoCrMo alloy whereas Figure 4.5 (b) exhibits smooth and uniform DLC on CoCrMo alloy substrates with pre-deposited diamond particles. These SEM images show that diamond incorporation can enhance adhesion of DLC on the CoCrMo alloys.

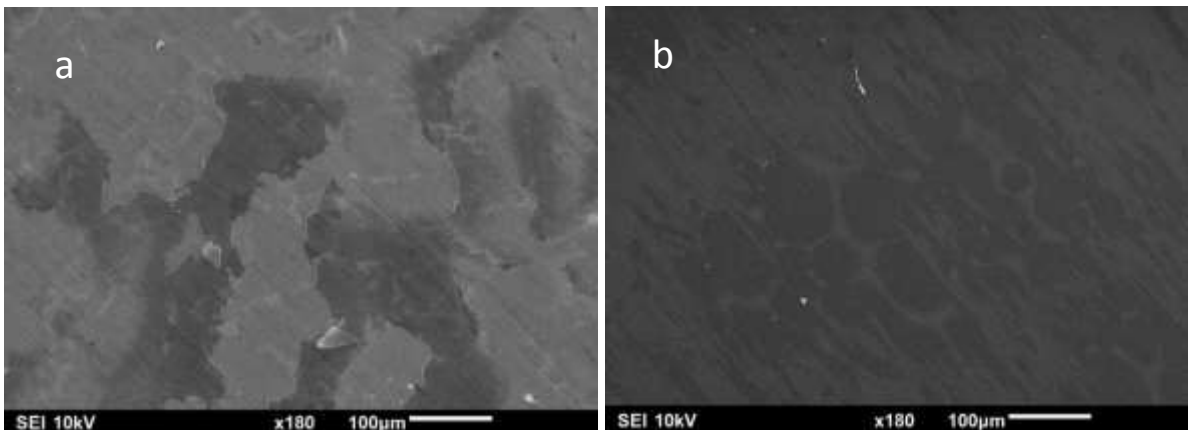


Figure 4.5 SEM images of (a) DLC delamination and (b) D-DLC on CoCrMo alloy

4.1.3 Surface Profilometry

Root Mean Squared (RMS) roughness of CoCrMo alloys with and without micro-diamond particles, DLC and NDLC coated alloys were measured by an optical profilometer. The RMS roughness value of mirror polished Cobalt alloy samples was 9.12 nm. After deposition of diamond-microparticles, the roughness value decreases to 6.17 nm. This roughness reduction might be resulted by the penetration of diamond particles at micro-cracks and grooves in the substrate surface resulting in a smooth and uniform film. However, DLC deposition on diamond particles slightly increased surface roughness to 7.96nm. This can be possible due to the initial energetic ion bombardment and existence C-H dangling bonds on the surface in a-C:H[93]. Nitrogen doping would reduce C-H dangling bonds and consequently decrease surface roughness. Figure 4.6 shows optical profilometer images with their corresponding RSM roughness values of bare and coated CoCrMo alloys.

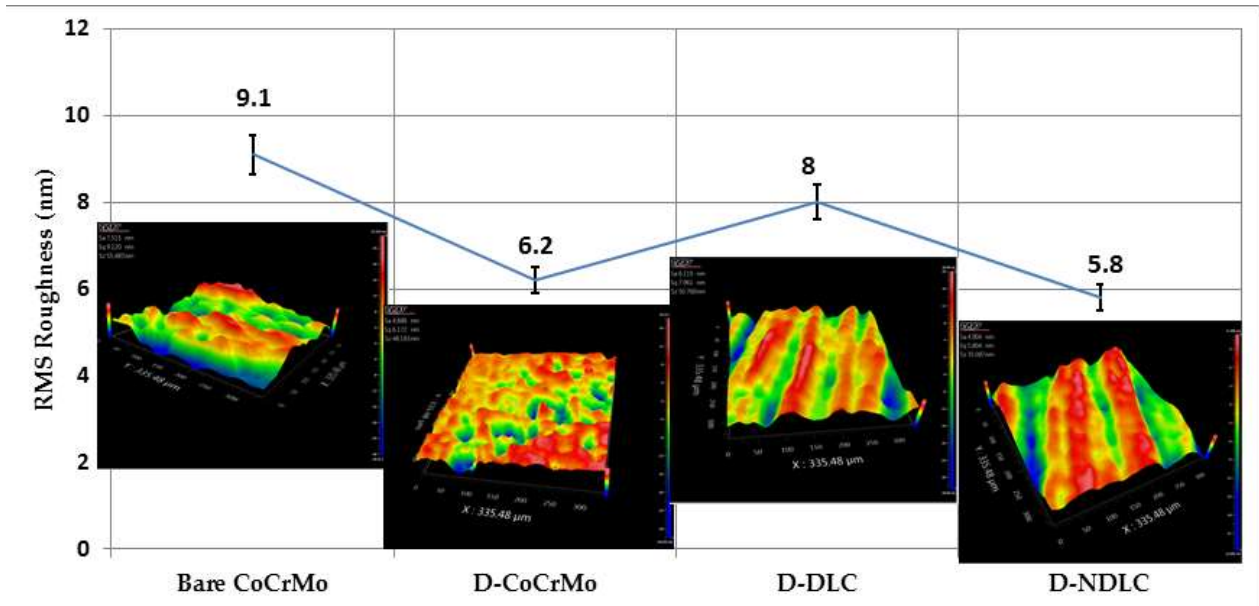


Figure 4.6 Surface Roughness of bare and coated CoCrMo alloys

4.1.4 Mechanical Properties

Hardness and Young's modulus values measured are shown in Table 4.1. DLC films presents the higher hardness and lower Young's modulus in comparison with bare CoCrMo and DLC coating doped with nitrogen. This is probably because nitrogen doping decreases the concentration of sp^3 bonds in the films, as shown in Fig.4.4. Consequently, hardness and Young's modulus decrease with nitrogen doping, similar trend has been reported previously [52].

Table 4.1 Hardness and Young's modulus of CoCrMo, DLC and D-NDLC coatings

Sample	Hardness (Gpa)	Young modulus (GPa)
CoCrMo	7.99 ± 0.4	258.63 ± 21.9
DLC	14.1 ± 0.2	124.7 ± 9.6
N-DLC-1	13.6 ± 0.4	131.6 ± 2.4

4.1.5 Adhesion

Figure 4.7 shows the SEM images of DLC and D-NDLC films after Rockwell C indentation testing. Spallation and cracking of the films are observed in the areas around the imprint, particularly on DLC sample in which severe delamination occurs (see Fig. 4.7a). Adhesion slightly increases with deposition of micro-diamond particles although the coating gradually peels off outwards from the center (see Fig. 4.7b). This adhesion improvement might be attributed to three main reasons: 1) the high interfacial bonding strength between micro-diamond particles and DLC due to its high chemical affinity, 2) strong mechanical interlocking to the amorphous carbon network[86,87], and it has been mentioned that depositing a fine grained diamond film can reduce surface tension and improve DLC adhesion[96]. Figure 4.7c shows a significant adhesion improvement on nitrogen doped DLC coatings. DLC adhesion increases considerably under the appropriate deposition conditions and Nitrogen content by increasing sp^2 chemical bonding in the film, as shown in the Raman spectra (see Figure 4.4). It has been reported that promoting sp^2 content by Nitrogen doping reduces the average coordination number of the amorphous carbon network and consequently reduces the internal stress[58]. The results have demonstrated that diamond incorporation and nitrogen doping can increase DLC adhesion to CoCrMo alloys.

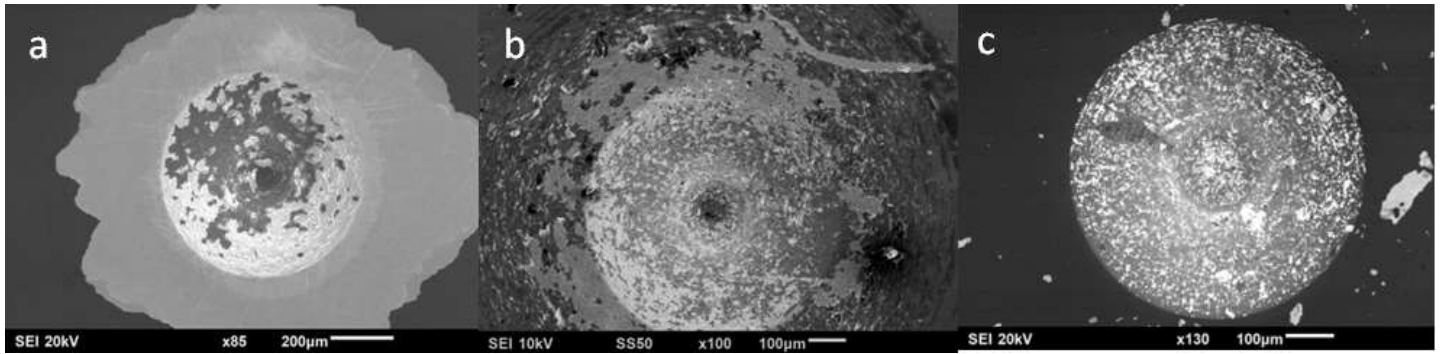


Figure 4.7 SEM images after Rockwell C indentation of (a) DLC on bare CoCrMo alloy, (b) D-DLC on CoCrMo alloy and (c) D-NDLC on CoCrMo alloy

4.2 Effect of nitrogen content on tribological properties of D/NDLC films on CoCrMo substrates

The previous section showed how the combination of micro-diamond particles and nitrogen doping into DLC increases adhesion significantly, reduces hardness and surface roughness of DLC films. This section presents a detailed X-Ray Photoelectron analysis of the chemical bonding of NDLC films that further explains the improvement in adhesion, mechanical properties and tribological behavior with different nitrogen concentrations.

4.2.1 Chemical Bonding and Structural Characterization

4.2.1.1 Raman Spectra nitrogen doped DLC films

Raman spectra of diamond-like carbon materials are strongly influenced by G (graphite) peak located at 1580cm^{-1} and D (disorder) peak at 1350cm^{-1} because of the scattering sp^2 sites even for tetrahedral amorphous carbons (less than 15% of sp^2 content)[35]. G peak arises from the stretching vibrations of sp^2 C=C chains or aromatic rings. On the other hand, breathing vibrations of sp^2 sites in rings are responsible for the presence of D peak[97].

Raman spectra of N-DLC coatings on silicon and CoCrMo are presented in Figure 4.8 and Figure 4.9, respectively. In the preparation of NDLC coatings, the gas flow rate of nitrogen was

increased gradually at 4 sccm, 8 sccm, 12 sccm, and 14 sccm while the other process parameters were kept constant as shown in Table 3.1. In order to obtain I_D/I_G ratio for each sample, all the Raman spectra were fitted by Wire 3.3 software using Gaussian-Lorentzian function. While increasing nitrogen content from 4sccm to 14sccm, G peak positions were found at 1524 cm^{-1} , 1526 cm^{-1} , 1527 cm^{-1} and 1528 cm^{-1} , corresponding to I_D/I_G ratios of 0.51, 0.68, 0.71 and 0.89, respectively as shown Figure 4.8.

The same tendency can be observed in Figure 4.9, indicating that sp^2 content in the film increases in parallel with the increase of nitrogen content. G peaks positions were located at 1527 cm^{-1} , 1528 cm^{-1} , 1528 cm^{-1} and 1530 cm^{-1} , corresponding to I_D/I_G ratios of 0.67, 0.82, 1.21 and 1.38, respectively. Nitrogen incorporation might facilitate clustering of sp^2 chemical species into carbonaceous rings (instead of chains) since the intensity of the disorder “D” peak is strongly influenced by the breathing vibration of aromatic rings [89–91]. The shifting of G peak positions in both spectra might be attributed to the increase in the bond disorder of the film by Nitrogen doping. This suggests that N doping causes a slight transition from sp^3 to sp^2 bonding vibrations in DLC films as reported previously by Hauert et al., and Hu et al. [47,93].

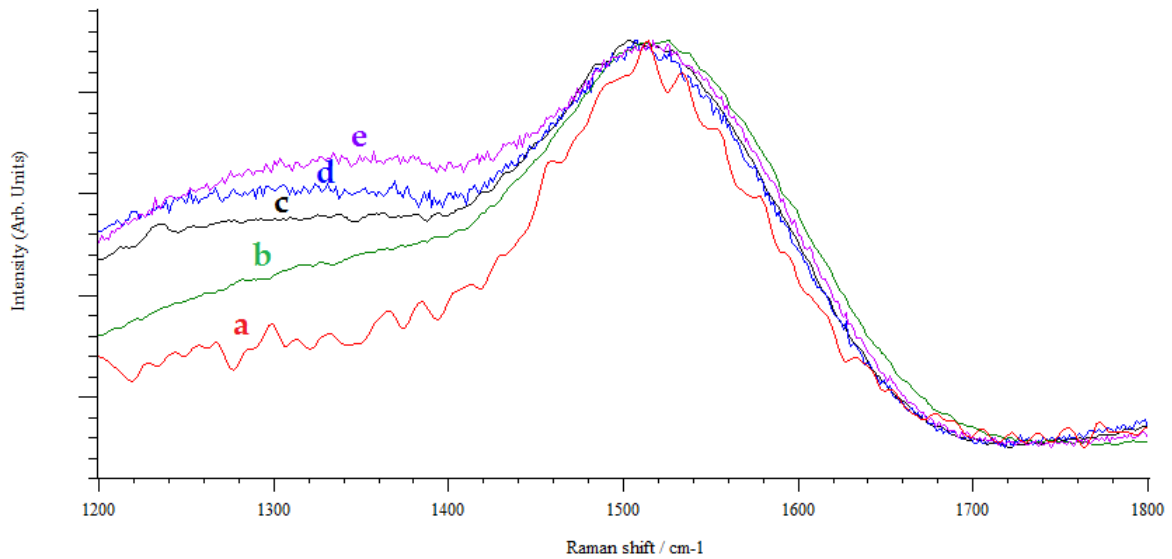


Figure 4.8 Raman spectra NDLC coatings on silicon with a) 0sccm, b) 4sccm, c) 8sccm, d) 12 sccm and e)16 sccm Nitrogen flow rate

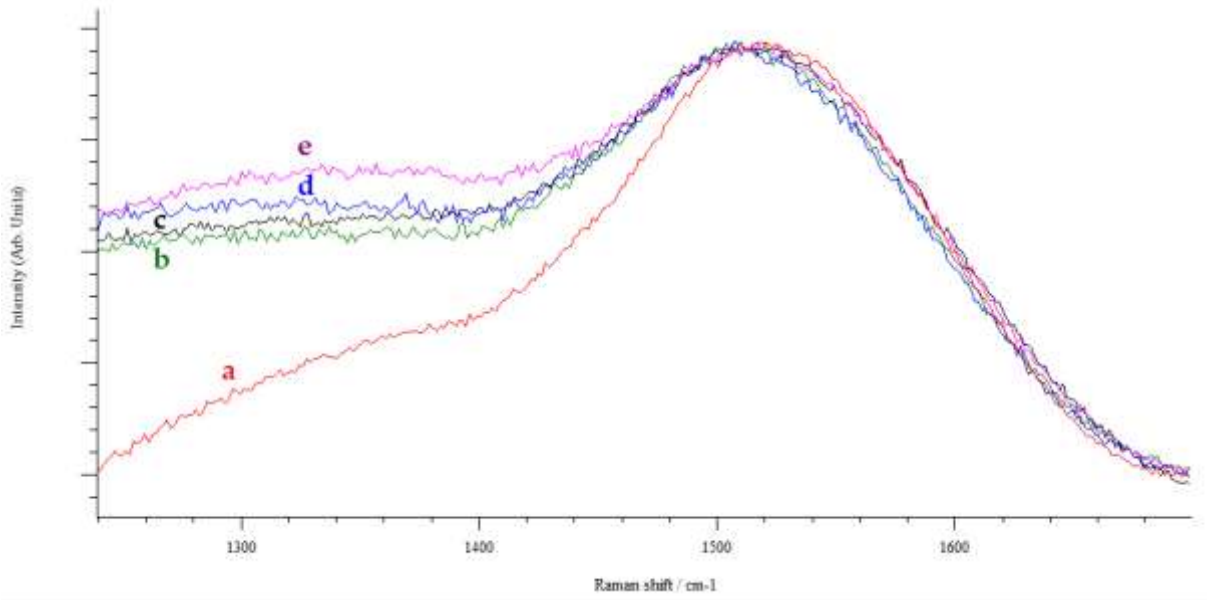


Figure 4.9 Raman spectra NDLC coatings on micro-diamond CoCrMo alloys with a) 0sccm, b) 4sccm, c) 8sccm, d) 12 sccm and e)16 sccm Nitrogen flow rate

4.2.1.2 XPS of nitrogen doped DLC films

CasaXPS software was used to de-convolute the XPS spectra using Gaussian-Lorentzian function. Figure 4.10 shows the deconvoluted C1s XPS spectra of DLC on silicon. The highest peak corresponds to C-C at 285.64 eV indicating a high sp^3 concentration in the sample confirming the results of the Raman spectra. The two other peaks at 284.97 eV and 286.78 eV correspond to C=C and C-N, respectively. Interestingly, C-N peak appeared at 286.78 eV in the spectra as a sign of contamination in the chamber, oxygen is more common to find as a contaminant [73] nevertheless the typical oxygen shoulder at 288.2 eV appears in the C1s spectra of D-NDLC-1 sample (see Figure 4.11a).

It can be seen in Figure 4.11a that at a low concentration of nitrogen doped DLC the sp^2 C=C peak at 284.92 eV is higher than the sp^3 C-C at 285.46 eV, but the C=N at 286.01 eV content is slightly lower than C-N at 286.72 eV. On the other hand, Fig.4.11b shows higher content of both C=C and C=N at 284.95 eV and 285.96 eV, respectively. This confirms that nitrogen doping increases the sp^2 concentration of the amorphous carbon films. Figure 4.12 shows the XPS

spectra in N1s of D-NDLC-1 (Figure 4.12a) and D-NDLC-4 (Figure 4.12b). In Figure 4.12b is confirmed that the higher the nitrogen incorporation the formation of sp^2 C=N at 400.71 eV is more favorable instead of sp^3 C-N at 399.25 eV. Table 4.2 summarizes the binding energies for C1s and N1s of DLC, D-NDLC-1, and D-NDLC-4.

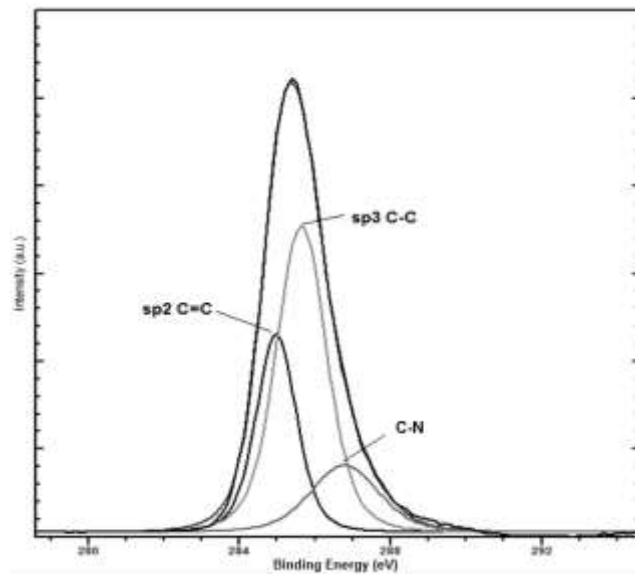


Figure 4.10 XPS C1s spectra of DLC on silicon

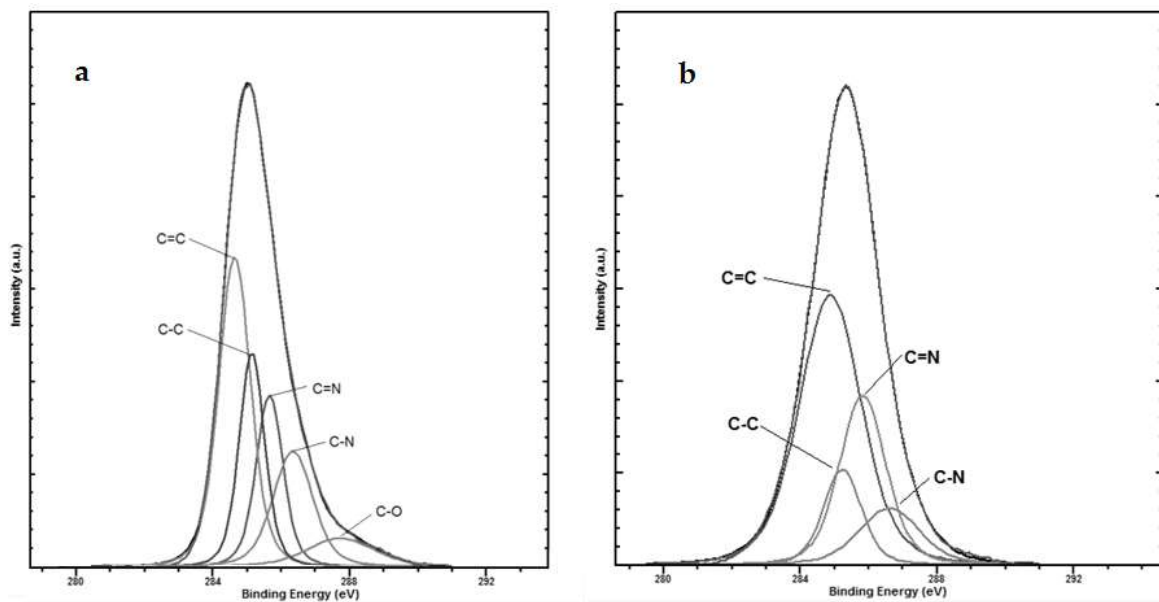


Figure 4.11 De-convolution of C1s XPS spectra of a) D-NDLC-1, and b) D-NDLC-4

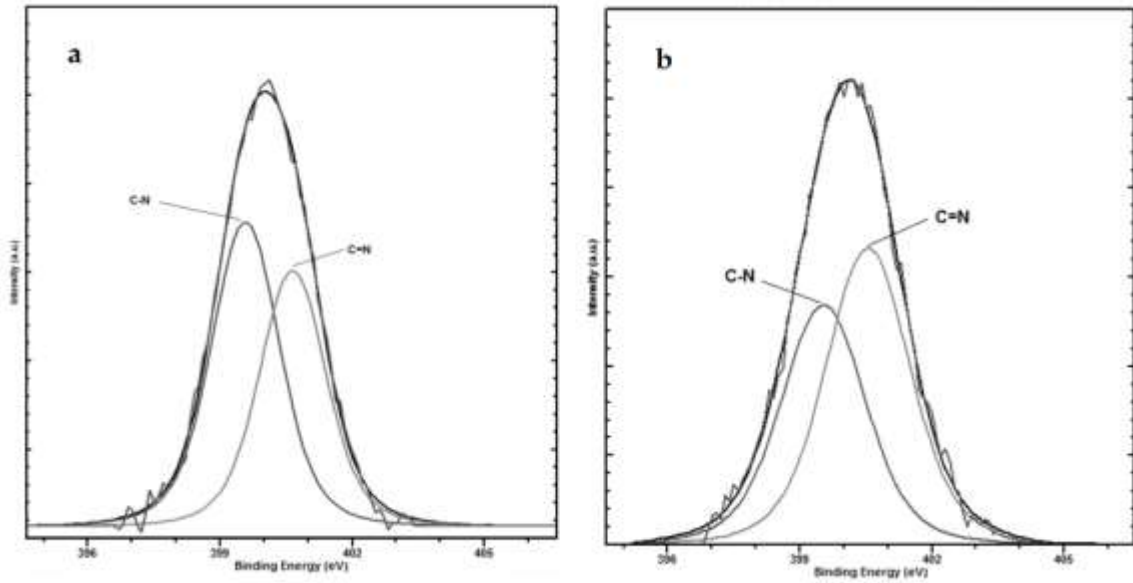


Figure 4.12 De-convolution of N1s XPS spectra of a) D-NDLC-1, and b) D-NDLC-4

Table 4.2. Binding energies of the different chemical states on DLC, D-NDLC-1, and D-NDLC-4.

XPS Line	Sample	Chemical state	Binding Energy (eV)	Ratio
C 1s	DLC	C=C	284.97	1
		C-C	285.64	1.93
		C-N	286.78	0.57
	D-NDLC-1	C=C	284.92	2.16
		C-C	285.46	1.18
		C=N	286.01	0.97
		C-N	286.72	1
	D-NDLC-4	C-O	288.21	0.4
		C=C	284.95	1
		C-C	285.37	0.22
C-N		286.82	0.21	
N 1s	D-NDLC-1	C-N	399.56	1
		C=N	400.63	0.82
	D-NDLC-4	C-N	399.25	1
		C=N	400.71	1.24

4.2.2 Surface Topography

Some external factors can affect roughness such as surface preparation of samples prior deposition, energy of the ion bombardment during deposition and chemical structure in the surface. In order to reduce the effect of these factors all the alloys were mirror polished under the same conditions prior diamond incorporation, the process parameters were kept constant during deposition. Figure 4.13 shows RMS roughness values of DLC, nitrogen doped DLC films on diamond CoCrMo specimens. It can be seen that the increase on nitrogen content lowers the surface roughness. This can be due to the enhancement of surface migration of the adatoms during deposition[90] and/or reduction on sp^3 C-H dangling bonds[93] by nitrogen doping.

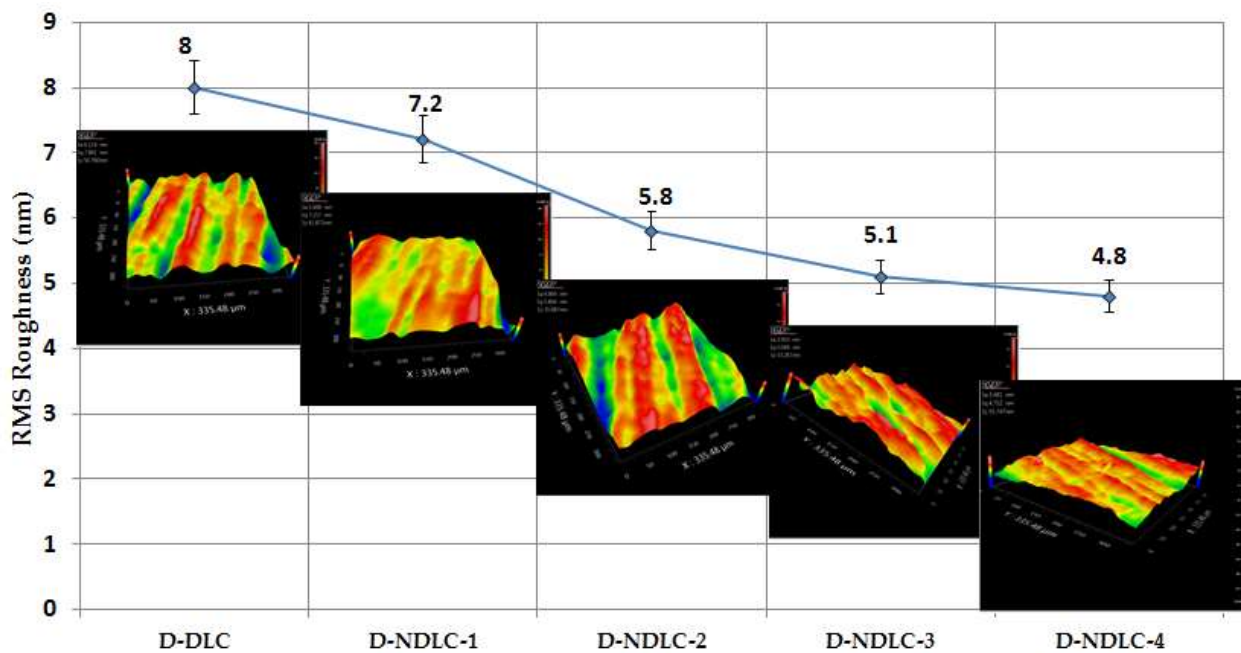


Figure 4.13 RMS Roughness of DLC and nitrogenated DLC films on CoCrMo alloys

4.2.3 Mechanical Properties

Hardness and Young's modulus are shown in Table 4.3. DLC films present the highest hardness among the other coatings. This is probably because before nitrogen incorporation the concentration of sp^3 chemical bond was higher as it was observed in previous Raman spectra and XPS analysis. DLC contains sp^3 C-C bonds and high amount of hydrogen in comparison with NDLC, hydrogen can increase sp^3 content by saturating sp^2 C=C bonds into sp^3 -CH₃. On the other hand, Nitrogen-doped coatings exhibit lower hardness, which is probably due to its higher sp^2 C=N bonding concentration as shown in Figure 4.12.

Table 4.3. Hardness, Young's modulus of CoCrMo, DLC and ND-NDLC coatings

Sample	Hardness (Gpa)	Young modulus (GPa)
CoCrMo	7.9 ± 0.4	258.6 ± 21.9
DLC	14.1 ± 0.2	124.7 ± 9.6
D-NDLC-1	13.6 ± 0.4	131.6 ± 2.4
D-NDLC-2	13.2 ± 0.6	134.5 ± 8.7
D-NDLC-3	12.5 ± 0.5	135.7 ± 4.5
D-NDLC-4	11.8 ± 0.3	141.6 ± 4.5

4.2.4 Adhesion

Rockwell C indentation testing was conducted at a load of 1470 N to evaluate qualitatively the adhesion of microdiamond and nitrogen incorporation on DLC thin films grown on CoCrMo. Figure 4.14 shows the SEM images of D-N-DLC films after Rockwell C indentation testing. Spallation and cracking of the films are observed in the areas around the imprint, particularly on DLC sample in which severe delamination indicates poor adhesion (see Fig. 4.14a). However, the spallation and cracking area decreases gradually as the concentration of nitrogen increases. Slight spallation can be observed on samples D-NDLC-1, D-NDLC-2. Still some microcracks can be observed on D-NDLC-3 sample. Delamination of DLC films occurs when the elastic energy stored in the film reaches a critical value which is closely

related with a critical film thickness. The adhesion improvement by nitrogen doping can be explained by Griffith's law [103]

$$\frac{h_f \sigma_f^2}{2E_f} \leq 2\gamma \quad (4.1)$$

where γ the surface fracture energy per unit area necessary to break the interface, h_f is film thickness, compressive stress and elastic modulus in the film are given by σ_f and E_f , respectively. When both sides of the equation are equal the coating delaminates[103]. Compressive stress is introduced in the film during deposition due to the energetic ion bombardment which also expands the substrate surface for the sub-plantation process describe in chapter 2. While stress increases, the elastic energy in the coating increases as well.

Then shear forces in the interface of the coating and substrate starts delamination of the coating because the elastic energy exceeds the surface fracture energy. In Figure 4.14a DLC delaminates dramatically for the high residual stress in the coating. DLC adhesion improves significantly from Figure 4.14b to Figure 4.14e due to internal stress reduction by nitrogen incorporation which has been well documented before [40,55,96,97]. As shown in Table 4.3, Young modulus of NDLC films increases as the nitrogen content increases, this suggest that nitrogen doping allows elastic stretching of DLC film without exceeding the surface fracture energy. Furthermore, diamond particles deposited on CoCrMo alloy promotes a strong interface by mechanical interlocking and surface tension reduction.

The results indicate that the cooperation of both diamond particles on CoCrMo alloys and nitrogen doping can increase DLC adhesion to CoCrMo alloys. The results are consistent with previous work for DLC and NDLC on different substrates[65,84,95]. Nevertheless, different deposition techniques (low energy ion beam deposition) and different substrate materials (Ti alloy) were used and much less nitrogen was doped in the work reported by us previously. This study further suggests that increasing nitrogen content into DLC coatings up to 27 % can further increase the adhesion of DLC on CoCrMo without a significant change in hardness.

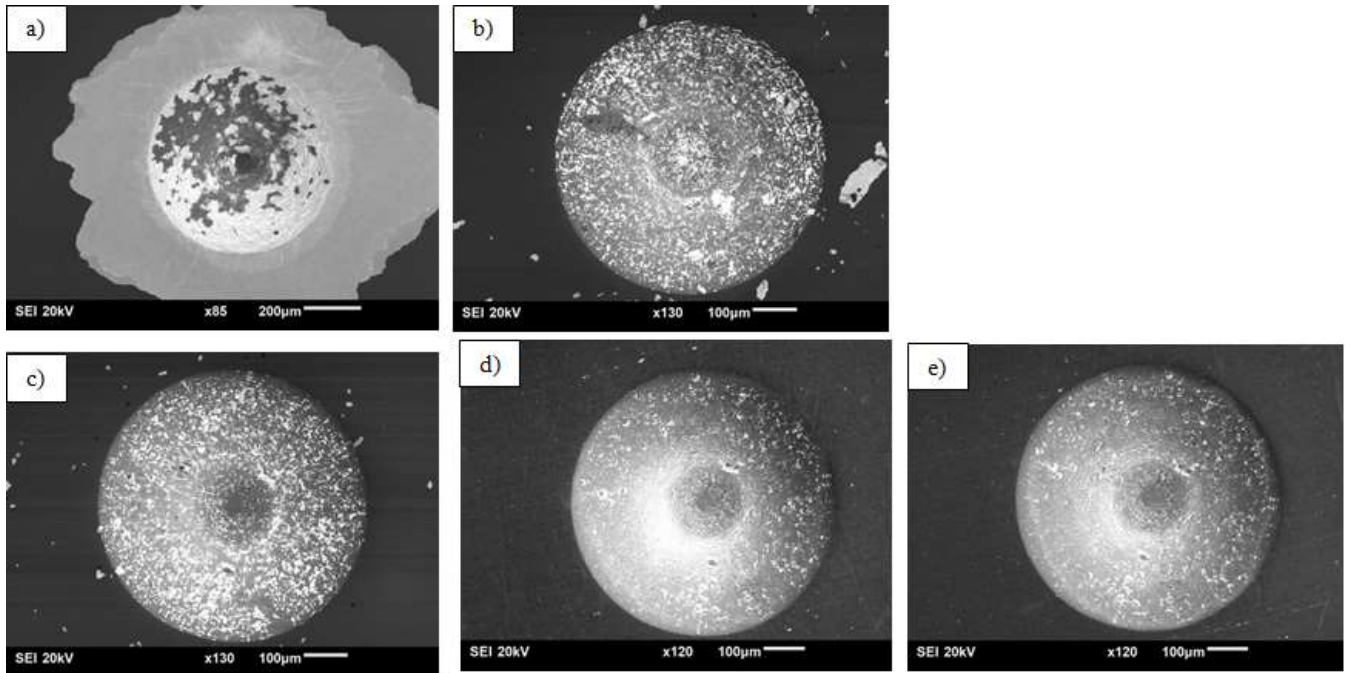


Figure 4.14 SEM images after Rockwell C indentation of a) DLC, b) D-DLC-1, c) D-NDLC-2, d) D-NDLC-3, and d) D-NDLC-4.

4.2.5 Friction and Wear

A Ball-on-disk configuration was used to study friction and wear of DLC and NDLC coatings on CoCrMo alloy specimens. All the samples were immersing in distilled water at room temperature. A constant load of 10 N was applied in a reciprocating motion at a constant speed of 5mm/sec. A total period of 10000 cycles was set to measure the Coefficient of friction (COF) of DLC and NDLC with ultra- high molecular weight polyethylene (UHMWPE) balls. No visible wear tracks of DLC and NDLC coatings against UHMWPE balls were found by using SEM microscope, suggesting very low wear from the coating.

The wear area from the polyethylene balls was measured by optical microscope in order to calculate the volume loss and wear rate of polyethylene balls. COF values decreased as the nitrogen content increased. The highest COF value of 0.21 was observed for DLC coatings. The COF measured were 0.16, 0.13, 0.12, 0.11 for 4 sccm, 8 sccm, 12 sccm and 14 sccm nitrogen flow rate samples. The results suggest that COF values decrease as the nitrogen content increase

probably due the reduction of sp^3 C-H dangling bonds as discussed in XPS results, and smoother surface as observed in Figure 4.13.

Wear tracks for UHMWPE balls on D-DLC and D-NDLC-4 samples are shown in Figure 4.16. The reduction in the width of the wear tracks from $800\mu\text{m}$ to $638\mu\text{m}$ shows the volume loss from UHMWPE balls. The removal of a material during contact with another material, depends on adhesion, hardness, abrasion or oxidation[35]. Since the UHMWPE balls are softer than DLC coatings the wear is more severe for UHMWPE balls. Table 4.4 shows the average wear rates for UHMWPE balls on DLC and N-DLC coatings. Nitrogen doping reduces sp^3 bonds in the film which are responsible for the hardness of DLC. With the reduction of hardness and surface roughness in NDLC coatings the wear rate of UHMWPE balls decreases which is beneficial for hip joint replacement application.

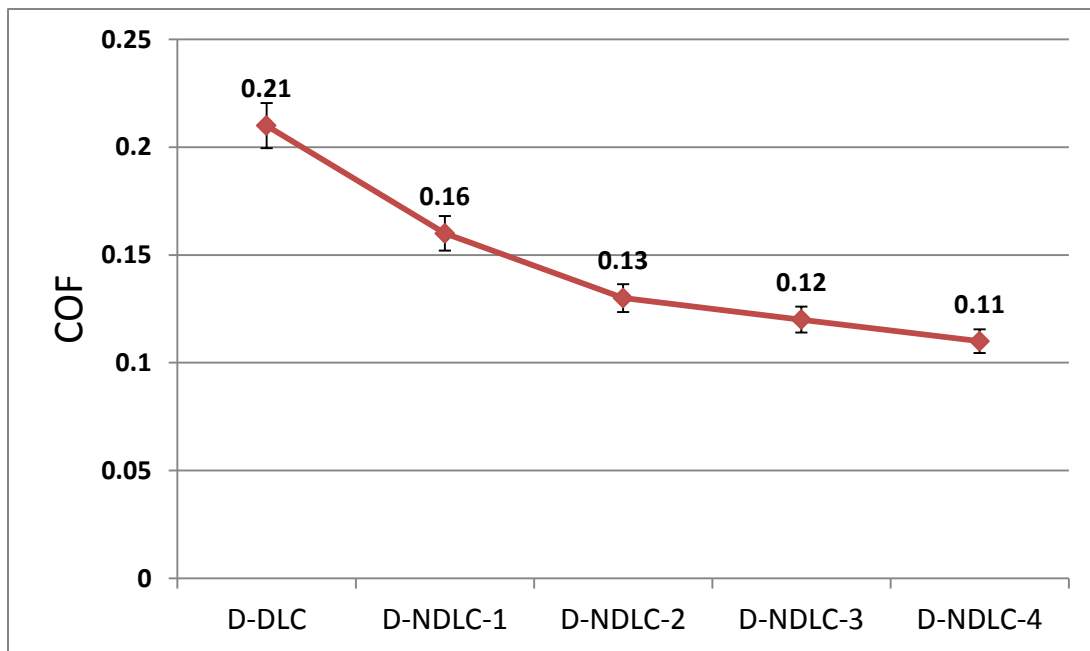


Figure 4.15 Coefficient of Friction of DLC and NDLC films against UHMWPE balls.

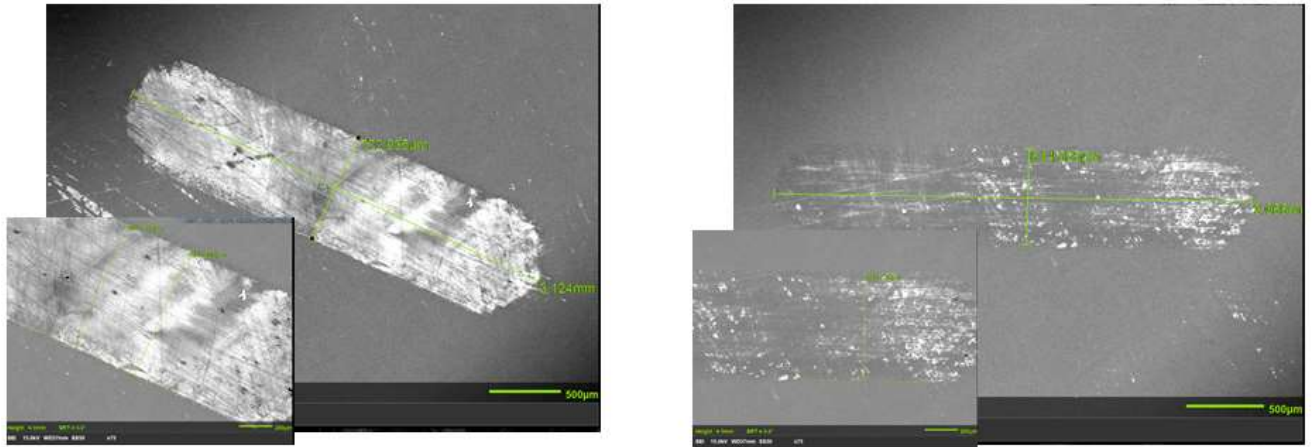


Figure 4.16 SEM images of wear tracks on D-DLC and D-NDLC-4 samples, the white areas correspond to UHMWPE balls loss

Table 4.4 Wear rate values for UHMWPE balls against DLC and NDLC coatings

Sample	Average wear rates ($\times 10^{-5} \text{ mm}^3/\text{Nm}$)
D-DLC	4.6 ± 0.2
D-NDLC-1	3.2 ± 0.1
D-NDLC-2	2.2 ± 0.1
D-NDLC-3	1.1 ± 0.2
D-NDLC-4	1.7 ± 0.1

CHAPTER 5 - CONCLUSIONS AND FUTURE WORK RECOMMENDATIONS

5.1 Summary and Conclusions

The mechanical and tribological properties of DLC thin films deposited on CoCrMo alloys by plasma enhanced chemical vapor deposition were investigated using different advanced techniques. The effects of diamond and nitrogen incorporation on adhesion enhancement of DLC alloy have been studied. The results and conclusions are summarized as follows:

1. Pure DLC coatings on untreated CoCrMo alloy presented severe delamination. Both diamond and nitrogen incorporation into DLC increase the adhesion of DLC coatings on the alloy.
2. Increasing doping concentration of nitrogen into the film promotes sp^2 C=N bonding which results in the increase of DLC adhesion.
3. Nitrogen doping reduces sp^3 C-C and sp^3 C-H bonds in the DLC films and thus decreases the roughness and hardness but increases the Young's Modulus of the films.
4. Increasing the nitrogen content in the film decreases the COF of the films sliding against UHMWPE balls and the wear rates of UHMWPE balls.
5. The incorporation of diamond and nitrogen into DLC improves the adhesion and decreases the COF and wear rates of the polymer balls, demonstrating that diamond and nitrogen incorporated DLC on CoCrMo alloy is very promising for hip joint replacement.

5.3 Future work

In the present study it has shown that microdiamond and nitrogen incorporation successfully improved DLC adhesion on CoCrMo alloy and wear rates of polyethylene balls were decreased. Since this combination is very promising for hip joint replacement, further systematic research on the process parameters is suggested to optimize the chemical structure of the coating for higher improvement on desire properties. The following future work is suggested:

1. It is important to investigate mechanical and tribological properties under simulated conditions as close as the ones in real service. Systematic studies of adhesion after immersion in simulated body fluid such as phosphate-buffered saline (PBS) solution over time is suggested to mimic an in-vivo environment.
2. Detail X-ray Photoelectron Spectroscopy analysis of N-DLC after immersion in PBS solution over time would reveal chemical changes in the surface of the film.
3. Friction and Wear studies of N-DLC under PBS solution at 37°C in order to simulate the conditions of the hip joint implant in its in vivo performance.
4. Corrosion analysis of N-DLC in PBS solution would disclose if nitrogen incorporation affects the chemical inertness of DLC.

REFERENCES

- [1] P. G. Collin, A. V D'Antoni, M. Loukas, R. J. Oskouian, and R. S. Tubbs, "Hip fractures in the elderly-: A Clinical Anatomy Review.," *Clin. Anat.*, vol. 97, no. August 2016, pp. 89–97, 2016.
- [2] T. D. Galsworthy, "Osteoporosis: Statistics, intervention, and prevention," *Ann.NY Acad.Sci.*, vol. 736, pp. 158–164, 1994.
- [3] F. Borgström, I. Lekander, M. Ivergard, O. Ström, A. Svedbom, V. Alekna, M. L. Bianchi, P. Clark, M. D. Curiel, H. P. Dimai, M. Jürisson, R. Kallikorm, O. Lesnyak, E. McCloskey, E. Nassonov, K. M. Sanders, S. Silverman, M. Tamulaitiene, T. Thomas, A. N. A. Tosteson, B. Jönsson, and J. A. Kanis, "The International Costs and Utilities Related to Osteoporotic Fractures Study (ICUROS) - Quality of life during the first 4 months after fracture," *Osteoporos. Int.*, vol. 24, no. 3, pp. 811–823, 2013.
- [4] M. G. Zywiell, S. A. Sayeed, A. J. Johnson, T. P. Schmalzried, and M. A. Mont, "Survival of hard-on-hard bearings in total hip arthroplasty: A systematic review," *Clin. Orthop. Relat. Res.*, vol. 469, no. 6, pp. 1536–1546, 2011.
- [5] Y. Liao, E. Hoffman, M. Wimmer, A. Fischer, J. Jacobs, and L. Marks, "CoCrMo metal-on-metal hip replacements.," *Phys. Chem. Chem. Phys.*, vol. 15, no. 3, pp. 746–56, 2013.
- [6] J. Corona-Gomez, X. Chen, and Q. Yang, "Effect of Nanoparticle Incorporation and Surface Coating on Mechanical Properties of Bone Scaffolds: A Brief Review," *J. Funct. Biomater.*, vol. 7, no. 3, p. 18, 2016.
- [7] F. Z. Cui and D. J. Li, "A review of investigations on biocompatibility of diamond-like carbon and carbon nitride films," *Surf. Coatings Technol.*, vol. 131, pp. 481–487, 2000.
- [8] G. Dearnaley and J. H. Arps, "Biomedical applications of diamond-like carbon (DLC) coatings: A review," *Surf. Coatings Technol.*, vol. 200, no. 7, pp. 2518–2524, 2005.
- [9] W. H. Liao, C. R. Lin, D. H. Wei, Y. R. Shen, Y. C. Li, J. A. Lee, and C. Y. Liang, "Concurrent improvement in biocompatibility and bioinertness of diamond-like carbon films with nitrogen doping," *J. Biomed. Mater. Res. - Part A*, 2012.
- [10] H. Holeczek, C. B. Santos, L. Haubold, and M. Metzner, "IFMBE Proceedings 2504 - DLC-Coated CoCrMo Steel for Use in Medical Implants – Wear and Corrosion Resistance Influence of Different Surface Finishing Techniques," pp. 1800–1803, 2009.
- [11] D. F. Franceschini, C. A. Achete, and F. L. Freire, "Internal stress reduction by nitrogen incorporation in hard amorphous carbon thin films," *Appl. Phys. Lett.*, vol. 60, no. 26, pp.

- 3229–3231, 1992.
- [12] B. Masahito, “Internal Stress of Hydrogenated Diamond-Like Carbon Films,” in *Diamond-Like Carbon Films*, Y. S. Tanaka, Ed. Miyashiro, Saitama, Japan: Nova Science, 2012, pp. 95–118.
- [13] P. Wang, X. Wang, T. Xu, W. Liu, and J. Zhang, “Comparing internal stress in diamond-like carbon films with different structure,” *Thin Solid Films*, vol. 515, no. 17, pp. 6899–6903, 2007.
- [14] C. Wei and C. H. Chen, “The effect of thermal and plastic mismatch on stress distribution in diamond like carbon film under different interlayer/substrate system,” *Diam. Relat. Mater.*, vol. 17, no. 7–10, pp. 1534–1540, 2008.
- [15] C. Wei, J. F. Yang, and F. C. Tai, “The stress reduction effect by interlayer deposition or film thickness for diamond like carbon on rough surface,” *Diam. Relat. Mater.*, vol. 19, no. 5–6, pp. 518–524, 2010.
- [16] G. H. Zhao, R. E. Aune, and N. Espallargas, “Tribocorrosion studies of metallic biomaterials: The effect of plasma nitriding and DLC surface modifications,” *J. Mech. Behav. Biomed. Mater.*, vol. 63, pp. 100–114, 2016.
- [17] H. Liu, Y. Leng, J. Tang, S. Wang, D. Xie, H. Sun, and N. Huang, “Tribological performance of ultra-high-molecular-weight polyethylene sliding against DLC-coated and nitrogen ion implanted CoCrMo alloy measured in a hip joint simulator,” *Surf. Coatings Technol.*, vol. 206, no. 23, pp. 4907–4914, 2012.
- [18] T. F. Zhang, B. Liu, B. J. Wu, J. Liu, H. Sun, Y. X. Leng, and N. Huang, “The stability of DLC film on nitrided CoCrMo alloy in phosphate buffer solution,” *Appl. Surf. Sci.*, vol. 308, pp. 100–105, 2014.
- [19] U. Müller, C. V. Falub, G. Thorwarth, C. Voisard, and R. Hauert, “Diamond-like carbon coatings on a CoCrMo implant alloy: A detailed XPS analysis of the chemical states at the interface,” *Acta Mater.*, vol. 59, no. 3, pp. 1150–1161, 2011.
- [20] C. Z. Zhang, Y. Tang, Y. S. Li, and Q. Yang, “Adhesion enhancement of diamond-like carbon thin films on Ti alloys by incorporation of nanodiamond particles,” *Thin Solid Films*, vol. 528, pp. 111–115, 2013.
- [21] S. Bhattacharjee, H. Niakan, Q. Yang, Y. Hu, and J. Dynes, “Enhancement of adhesion and corrosion resistance of diamond-like carbon thin films on Ti-6Al-4V alloy by nitrogen doping and incorporation of nanodiamond particles,” *Surf. Coatings Technol.*, vol. 284, pp.

- 153–158, 2015.
- [22] D. Bootkul, B. Supsermpol, N. Saenphinit, C. Aramwit, and S. Intarasiri, “Nitrogen doping for adhesion improvement of DLC film deposited on Si substrate by Filtered Cathodic Vacuum Arc (FCVA) technique,” *Appl. Surf. Sci.*, vol. 310, pp. 284–292, 2014.
- [23] Z. Seker, H. Ozdamar, M. Esen, R. Esen, and H. Kavak, “The effect of nitrogen incorporation in DLC films deposited by ECR Microwave Plasma CVD,” *Appl. Surf. Sci.*, vol. 314, pp. 46–51, 2014.
- [24] Keck Medicine of USC, “Hip joint replacement.” [Online]. Available: <http://keckmedicine.adam.com/graphics/images/en/23246.jpg>. [Accessed: 25-Apr-2017].
- [25] Carpenter Technology Corp., “Certificate of Tests CoCrMo, Cert Serial 001002737.” .
- [26] P. Samyn and G. Schoukens, “The lubricity of graphite flake inclusions in sintered polyimides affected by chemical reactions at high temperatures,” *Carbon N. Y.*, vol. 46, no. 7, pp. 1072–1084, 2008.
- [27] N. Deprez and D. S. McLachlan, “The analysis of the electrical conductivity of graphite conductivity of graphite powders during compaction,” *J. Phys. D. Appl. Phys.*, vol. 21, no. 1, pp. 101–107, 1988.
- [28] J. C. Angus, F. A. Buck, M. Sunkara, T. F. Groth, C. C. Hayman, and R. Gat, “Diamond growth at low pressures,” *MRS Bull.*, vol. 14, no. 10, pp. 38–47, 1989.
- [29] M. Schwander and K. Partes, “A review of diamond synthesis by CVD processes,” *Diam. Relat. Mater.*, vol. 20, no. 9, pp. 1287–1301, 2011.
- [30] W. Fan, L. Zhang, and T. Liu, “Graphene-Carbon Nanotube Hybrids for Energy and Environmental Applications,” pp. 1–19, 2017.
- [31] B. Dischler, “Handbook of Spectral Lines in Diamond,” pp. 413–414, 2012.
- [32] J. Robertson, “Amorphous carbon,” *Adv. Phys.*, vol. 60, no. 1, pp. 87–144, 2011.
- [33] M. Scarselli, P. Castrucci, and M. De Crescenzi, “Electronic and optoelectronic nano-devices based on carbon nanotubes,” *J. Phys. Condens. Matter*, vol. 24, 2012.
- [34] J. Robertson, “Amorphous carbon,” *Curr. Opin. Solid State Mater. Sci.*, vol. 1, no. 4, pp. 557–561, 1996.
- [35] J. Robertson, “Diamond-like amorphous carbon,” *Mater. Sci. Eng. R Reports*, vol. 37, no. 4–6, pp. 129–281, 2002.
- [36] D. R. McKenzie, “Tetrahedral bonding in amorphous carbon,” *Reports Prog. Phys.*, vol. 59, no. 12, pp. 1611–1664, 1999.

- [37] A. Erdemir and C. Donnet, "Tribology of diamond-like carbon films: recent progress and future prospects," *J. Phys. D. Appl. Phys.*, vol. 39, no. 18, pp. R311–R327, 2006.
- [38] S. Aisenberg and R. Chabot, "Ion-beam deposition of thin films of diamondlike carbon," *J. Appl. Phys.*, vol. 42, no. 7, pp. 2953–2958, 1971.
- [39] F. Stevie, "Focused Ion Beam Secondary Ion Mass Spectrometry (FIB-SIMS)," in *Introduction to Focused Ion Beams: Instrumentation, Theory, Techniques and Practice.*, Springer US, 2005, pp. 269–280.
- [40] H. G. Fuß and M. Frank, "Industrial production of DLC coatings," in *Tribology of Diamond-Like Carbon Films: Fundamentals and Applications*, Springer US., 2008, pp. 457–468.
- [41] A. Voevodin, S. Walck, J. Solomon, P. John, D. Ingram, M. Donley, and Zabinski., "Structure and properties of diamondlike carbon films produced by pulsed laser deposition," *J. Vac. Sci. Technol. A Vacuum, Surfaces Film.*, vol. 14, no. 3, pp. 1927–1932, 1996.
- [42] J. Robertson, "Properties of diamond-like carbon," *Surf. Coatings Technol.*, vol. 50, no. 3, pp. 185–203, 1992.
- [43] Y. Lifshitz, "Diamond-like carbon — present status," *Diam. Relat. Mater.*, vol. 8, no. 8–9, pp. 1659–1676, 1999.
- [44] J. Robertson, "The deposition mechanism of diamond-like a-C and a-C: H," *Diam. Relat. Mater.*, vol. 3, no. 4–6, pp. 361–368, 1994.
- [45] J. C. Angus and F. Jansen, "Dense 'diamondlike' hydrocarbons as random covalent networks," *J. Vac. Sci. Technol. A Vacuum, Surfaces Film.*, vol. 6, no. 3, pp. 1778–1782, 1988.
- [46] M. G. Of, "Metastable Growth of," 1991.
- [47] X. L. Peng and T. W. Clyne, "Residual Stress and Debonding of DLC Films on Metallic Substrates," *Diam. Relat. Mater.*, vol. 7, no. 7, pp. 944–950, 1998.
- [48] J. Fontaine, C. Donnet, and A. Erdemir, "Fundamentals of the tribology of DLC coatings," in *Tribology of Diamond-Like Carbon Films: Fundamentals and Applications*, Springer US, 2008, pp. 139–154.
- [49] C. Wei, Y. S. Wang, and F. C. Tai, "The role of metal interlayer on thermal stress, film structure, wettability and hydrogen content for diamond like carbon films on different substrate," *Diam. Relat. Mater.*, vol. 18, no. 2–3, pp. 407–412, 2009.

- [50] Y. Pauleau, "Residual Stress in DLC Films and Adhesion to Various Substrates," in *Tribology of Diamond-Like Carbon Films*, C. Donnet and A. Erdemir, Eds. Springer, 2008, pp. 104–107.
- [51] M. M. M. Bilek and D. R. McKenzie, "A comprehensive model of stress generation and relief processes in thin films deposited with energetic ions," *Surf. Coatings Technol.*, vol. 200, no. 14–15, pp. 4345–4354, 2006.
- [52] S. C. Ray, W. F. Pong, and P. Papakonstantinou, "Iron, nitrogen and silicon doped diamond like carbon (DLC) thin films: A comparative study," *Thin Solid Films*, vol. 610, pp. 42–47, 2016.
- [53] L. K. Cheah, X. Shi, J. R. Shi, E. J. Liu, and S. R. P. Silva, "Properties of nitrogen doped tetrahedral amorphous carbon films prepared by filtered cathodic vacuum arc technique," *J. Non. Cryst. Solids*, vol. 242, no. 1, pp. 40–48, 1998.
- [54] P. Navaneethkrishnan, S. Ganesh Sundara Raman, R. Gnanamoorthy, and N. Ravi, "Relative performance of hydrogenated, argon-incorporated and nitrogen-incorporated diamond-like carbon coated Ti-6Al-4V samples under fretting wear loading," *Thin Solid Films*, vol. 517, no. 15, pp. 4365–4371, 2009.
- [55] R. Hauert, A. Glisenti, S. Metin, J. Goitia, J. H. Kaufman, P. H. M. Van Loosdrecht, A. J. Kellock, P. Hoffmann, R. L. White, and B. D. Hermsmeier, "Influence of nitrogen doping on different properties of aC: H," *Thin Solid Films*, vol. 268, no. 1, pp. 22–29, 1995.
- [56] M. Cohen and A. Liu, "Structural properties and electronic structure of low-compressibility materials: beta -Si₃N₄ and hypothetical beta -C₃N₄," *Phys. Rev. B Condensed Matter*, vol. 41, no. 15, pp. 10727–10734, 1990.
- [57] N. P. Hellgren, E. Johansson, Mats P. E. Broitman, L. Hultman, and J.-E. Sundgren, "Role of Nitrogen in the Formation of Hard and Elastic CN X Thin Films by Reactive Magnetron Sputtering," *Phys. Rev. B - Condens. Matter Mater. Phys.*, vol. 59, no. 7, pp. 5162–5169, 1999.
- [58] S. Kumar, P. N. Dixit, D. Sarangi, and R. Bhattacharyya, "Possible solution to the problem of high built-up stresses in diamond-like carbon films," *J. Appl. Phys.*, vol. 85, no. 1999, p. 3866, 1999.
- [59] Y. S. Zou, Q. M. Wang, H. Du, G. H. Song, J. Q. Xiao, J. Gong, C. Sun, and L. S. Wen, "Structural characterization of nitrogen doped diamond-like carbon films deposited by arc ion plating," *Appl. Surf. Sci.*, vol. 241, no. 3–4, pp. 295–302, 2005.

- [60] A. Grill, "Tribology of diamondlike carbon and related materials: an updated review," *Surf. Coatings Technol.*, vol. 94, pp. 507–513, 1997.
- [61] Y. Kusano, J. E. Evetts, R. E. Somekh, and I. M. Hutchings, "Properties of carbon nitride films deposited by magnetron sputtering," *Thin Solid Films*, vol. 332, no. 1–2, pp. 56–61, 1998.
- [62] J. C. Sanchez-Lopez and A. Fernandez, "Doping and alloying effects on DLC coatings," in *Tribology of Diamond-Like Carbon Films: Fundamentals and Applications*, 2008, pp. 311–328.
- [63] E. N. Kaufmann, *Characterization of Materials*. Hoboken, NJ: John Wiley and Sons, 2003.
- [64] J. R. Ferraro, K. Nakamoto, and C. W. Brown, "Chapter 1 - Basic Theory," in *Introductory Raman Spectroscopy*, Second., San Diego: Academic Press, 2003, pp. 1–94.
- [65] S. Wang, J. Zhu, J. Wang, X. Yin, and X. Han, "Raman spectroscopy and mechanical properties of multilayer tetrahedral amorphous carbon films," *Thin Solid Films*, vol. 519, no. 15, pp. 4906–4909, 2011.
- [66] A. C. Ferrari, "Determination of bonding in diamond-like carbon by Raman spectroscopy," *Diam. Relat. Mater.*, vol. 11, no. 3–6, pp. 1053–1061, 2002.
- [67] J. Schwan, S. Ulrich, V. Batori, H. Ehrhardt, and S. R. P. Silva, "Raman spectroscopy on amorphous carbon films," *J. Appl. Phys.*, vol. 80, no. 1, pp. 440–447, 1996.
- [68] M. A. Tamor and W. C. Vassell, "Raman 'fingerprinting' of amorphous carbon films," *J. Appl. Phys.*, vol. 76, no. 6, pp. 3823–3830, 1994.
- [69] R. E. Whan, *ASM Handbook Volume 10: Materials Characterization*. ASM International, 1986.
- [70] Y. Tang, Y. S. Li, Q. Yang, and a. Hirose, "Characterization of hydrogenated amorphous carbon thin films by end-Hall ion beam deposition," *Appl. Surf. Sci.*, vol. 257, pp. 4699–4705, 2011.
- [71] N. W. Khun and E. Liu, "Enhancement of adhesion strength and corrosion resistance of nitrogen or platinum/ruthenium/nitrogen doped diamond-like carbon thin films by platinum/ruthenium underlayer," *Diam. Relat. Mater.*, vol. 19, no. 7–9, pp. 1065–1072, 2010.
- [72] P. Ashtijoo, S. Bhattacharjee, R. Sutarto, Y. Hu, and Q. Yang, "Fabrication and characterization of adherent diamond-like carbon based thin films on polyethylene

- terephthalate by end hall ion beam deposition,” *Surf. Coatings Technol.*, vol. 308, pp. 90–97, 2016.
- [73] E. Riedo, F. Comin, J. Chevrier, F. Schmithusen, S. Decossas, and M. Sancrotti, “Structural properties and surface morphology of laser-deposited amorphous carbon and carbon nitride films,” *Surf. Coatings Technol.*, vol. 125, no. 1–3, pp. 124–128, 2000.
- [74] W. C. Oliver and G. M. Pharr, “An improved technique for determining hardness and elastic modulus using load and displacement sensing indentation experiments.,” *J. Mater. Res.*, vol. 7, no. 6, pp. 1564–1583, 1992.
- [75] G. D. Quinn, R. K. Gettings, and L. Ives, “A standard reference material for vickers hardness of ceramics and Hardmetals,” in *IMEKO TC5 Conference on Hardness Measurements Theory and Application in Laboratories and Industries*, 2004, pp. 90–97.
- [76] J. A. Knapp, D. M. Follstaedt, S. M. Myers, J. C. Barbour, and T. A. Friedmann, “Finite-element modeling of nanoindentation,” *J. Appl. Phys.*, vol. 85, no. 3, pp. 1460–1474, 1999.
- [77] M. Weiler, S. Sattel, T. Giessen, K. Jung, H. Ehrhardt, V. Veerasamy, and J. Robertson, “Preparation and properties of highly tetrahedral hydrogenated amorphous carbon,” *Phys. Rev. B*, vol. 53, no. 3, pp. 1594–1608, 1996.
- [78] C. V. Falub, U. Müller, G. Thorwarth, M. Parlinska-Wojtan, C. Voisard, and R. Hauert, “In vitro studies of the adhesion of diamond-like carbon thin films on CoCrMo biomedical implant alloy,” *Acta Mater.*, vol. 59, no. 11, pp. 4678–4689, 2011.
- [79] Y. J. Won and H. Ki, “Effect of film gradient profile on adhesion strength, residual stress and effective hardness of functionally graded diamond-like carbon films,” *Appl. Surf. Sci.*, vol. 311, pp. 775–779, 2014.
- [80] L. F. Bonetti, G. Capote, L. V. Santos, E. J. Corat, and V. J. Trava-Airoldi, “Adhesion studies of diamond-like carbon films deposited on Ti6Al4V substrate with a silicon interlayer,” *Thin Solid Films*, vol. 515, no. 1, pp. 375–379, 2006.
- [81] Verein-Deutscher-Ingenieure, “Daimler Benz Adhesion Test, VDI 3198.” VDI-Verlag, Dusseldorf, p. 7, 1992.
- [82] W. Heinke, A. Leyland, A. Matthews, G. Berg, C. Friedrich, and E. Broszeit, “Evaluation of PVD nitride coatings, using impact, scratch and Rockwell-C adhesion tests,” *Thin Solid Films*, vol. 270, no. 1–2, pp. 431–438, 1995.
- [83] M. Zawischa, S. Makowski, N. Schwarzer, and V. Weihnacht, “Scratch resistance of superhard carbon coatings - A new approach to failure and adhesion evaluation,” *Surf.*

- Coatings Technol.*, vol. 308, pp. 341–348, 2016.
- [84] “Schematic of Scratch Test.” [Online]. Available: <http://www.adhesivestoolkit.com/Docs/test/MECHANICAL TEST METHOD 1 - Continued.xtp>. [Accessed: 21-Mar-2017].
- [85] T. Chudoba and F. Richter, “Investigation of creep behaviour under load during indentation experiments and its influence on hardness and modulus results,” *Surf. Coatings Technol.*, vol. 148, no. 2–3, pp. 191–192, 2001.
- [86] L. Ladani, E. Harvey, S. F. Choudhury, and C. R. Taylor, “Effect of Varying Test Parameters on Elastic-plastic Properties Extracted by Nanoindentation Tests,” *Exp. Mech.*, vol. 53, no. 8, pp. 1299–1309, 2013.
- [87] R. Goodall and T. W. Clyne, “A critical appraisal of the extraction of creep parameters from nanoindentation data obtained at room temperature,” *Acta Mater.*, vol. 54, no. 20, pp. 5489–5499, 2006.
- [88] W. C. Oliver and G. M. Pharr, “Measurement of hardness and elastic modulus by instrumented indentation: Advances in understanding and refinements to methodology,” *J. Mater. Res.*, vol. 19, no. 1, pp. 3–20, 2004.
- [89] T. F. Zhang, Q. Y. Deng, B. Liu, B. J. Wu, F. J. Jing, Y. X. Leng, and N. Huang, “Surface & Coatings Technology Wear and corrosion properties of diamond like carbon (DLC) coating on stainless steel , CoCrMo and Ti6Al4V substrates,” vol. 273, pp. 12–19, 2015.
- [90] T. F. Zhang, B. J. Wu, Q. Y. Deng, W. J. Huang, N. Huang, and Y. X. Leng, “Diamond & Related Materials Effect of a hydrogenated interface on the wear behavior of a diamond-like carbon film in a water environment,” vol. 74, pp. 53–58, 2017.
- [91] G. Zhao, R. E. Aune, and N. Espallargas, “Tribocorrosion studies of metallic biomaterials : The effect of plasma nitriding and DLC surface modifications,” vol. 63, pp. 100–114, 2016.
- [92] “ISO 14242-1:2002, Implants for surgery—wear of total hip-joint prostheses—part 1: loading and displacement parameters for wear-testing machines and corresponding environmental conditions for test.” International Organization for Standardization, 2002.
- [93] S. Srinivasan, Y. Tang, Y. S. Li, Q. Yang, and A. Hirose, “Ion beam deposition of DLC and nitrogen doped DLC thin films for enhanced haemocompatibility on PTFE,” *Appl. Surf. Sci.*, vol. 258, no. 20, pp. 8094–8099, 2012.
- [94] M. P. Larsson and M. M. Ahmad, “Improved polymer–glass adhesion through micro-

- mechanical interlocking,” *J. Micromechanics Microengineering*, vol. 16, no. 6, pp. S161–S168, 2006.
- [95] L. Q. Gou, X. L. Shi, X. M. Zhao, Y. Bai, and L. J. Qiao, “Composite diamond-DLC coated nanoprobe tips for wear resistance and adhesion reduction,” *Surf. Coatings Technol.*, vol. 206, no. 19–20, pp. 4099–4105, 2012.
- [96] F. Deuerler, H. Van Den Berg, R. Tabersky, A. Freundlieb, M. Pies, and V. Buck, “Pretreatment of substrate surface for improved adhesion of diamond films on hard metal cutting tools,” *Diam. Relat. Mater.*, vol. 5, no. 12, pp. 1478–1489, 1996.
- [97] A. C. Ferrari and J. Robertson, “Interpretation of Raman spectra of disordered and amorphous carbon,” *Phys. Rev. B*, vol. 61, no. 20, pp. 14095–14107, 2000.
- [98] F. Tuinstra and J. L. Koenig, “Raman Spectrum of Graphite,” *J. Chem. Phys.*, vol. 53, no. 3, pp. 1126–1130, 1970.
- [99] T. W. Scharf, R. D. Ott, D. Yang, and J. A. Barnard, “Structural and tribological characterization of protective amorphous diamond-like carbon and amorphous CN_x overcoats for next generation hard disks,” *J. Appl. Phys.*, vol. 85, no. 6, pp. 3142–3154, 1999.
- [100] K. Zhou, P. Ke, X. Li, Y. Zou, and A. Wang, “Microstructure and electrochemical properties of nitrogen-doped DLC films deposited by PECVD technique,” *Appl. Surf. Sci.*, vol. 329, pp. 281–286, 2015.
- [101] J. Hu, P. Yang, and C. Lieber, “Nitrogen-driven sp³ to sp² transformation in carbon nitride materials,” *Phys. Rev. B*, vol. 57, no. 6, pp. R3185–R3188, 1998.
- [102] Y. H. Yu, J. P. Zhao, X. Wang, S. Q. Yang, T. S. Shi, X. H. Liu, E. Z. Lou, J. B. Xu, and I. H. Wilson, “Surface morphology of nitrogen doped tetrahedral amorphous carbon films on silicon by atomic microscopy imaging,” *Mater. Lett.*, vol. 34, no. February, pp. 1–4, 1998.
- [103] P. Mosaner, M. Bonelli, and A. Miotello, “Pulsed laser deposition of diamond-like carbon films: Reducing internal stress by thermal annealing,” *Appl. Surf. Sci.*, vol. 208–209, no. 1, pp. 561–565, 2003.
- [104] G. . Franceschini, D.; Achete, C.; Freire, F.; Mariotto, “Internal Stress in Nitrogen Doped Diamond-Like A-C:H Films,” in *MRS Proceedings 270*, 1992, pp. 481–486.
- [105] V. Anita, T. Butuda, T. Maeda, K. Takizawa, N. Saito, and O. Takai, “Effect of N doping on properties of diamond-like carbon thin films produced by RF capacitively coupled chemical vapor deposition from different precursors,” *Diam. Relat. Mater.*, vol. 13, no.

11–12, pp. 1993–1996, 2004.

- [106] K. Ozeki and K. K. Hirakuri, “The effect of nitrogen and oxygen plasma on the wear properties and adhesion strength of the diamond-like carbon film coated on PTFE,” *Appl. Surf. Sci.*, vol. 254, no. 6, pp. 1614–1621, 2008.